SIAM J. APPL. MATH.
Vol. 76, No. 4, pp. 1606–1632

ANALYTICAL SOLUTION FOR SPHEROIDAL DROP UNDER AXISYMMETRIC LINEARIZED BOUNDARY CONDITIONS*

MICHAEL ZABARANKIN†

Abstract. A liquid spheroidal drop freely suspended in another fluid is considered under arbitrary axisymmetric boundary conditions, which are linearized with respect to the velocity field and can result, in particular, from an axisymmetric external flow and an electric field being applied either separately or in combination. All nonlinear effects including inertia and surface charge convection are assumed to be negligible, whereas the drop and the ambient fluid are assumed to be leaky dielectrics and to have different viscosities. Central to the analysis are the reformulated stress boundary conditions and representation of the velocity field inside and outside the drop in terms of non-Stokes stream functions. In the prolate spheroidal coordinates, the stream functions are expanded into infinite series of spheroidal harmonics, and the reformulated velocity and stress boundary conditions yield a first-order difference equation for the series coefficients, which admits an exact nonrecursive solution. "Steady" spheroidal drops then correspond to minimums of a kinematic condition error that admits a simple efficient approximation. Under the simultaneous presence of aligned linear flow and a uniform electric field with corresponding capillary numbers Ca and Ca_E, a spherical drop is stationary when $\mathrm{Ca} = k\,\mathrm{Ca}_E$ and becomes prolate/oblate when $\mathrm{Ca} \gtrless k\,\mathrm{Ca}_E$, where k is proportional to the Taylor discriminating function and depends on ratios of viscosities, dielectric constants, and electric conductivities of the two phases. A spheroidal drop is "steady" when $\mathrm{Ca} = k_1\,\mathrm{Ca}_E + k_2$, where k_1 and k_2 depend on the spheroid's axes ratio d and approach k and 0, respectively, as $d \to 1$. The results show that when the Taylor deformation parameter D is in the range $[-0.5, 0.4]$, this relationship can be used for finding any of the three Ca, Ca_E, and D when the other two are given.

Key words. Stokes flow, spheroidal drop, non-Stokes stream function, exact solution, electric field, linear flow

AMS subject classifications. 76D07, 76D45, 76W05

DOI. 10.1137/15M1048471

1. Introduction.

The problem of deformation and breakup of a liquid drop freely suspended in another fluid has been and continues to be of significant scientific interest due to its wide spectrum of applications ranging from classical emulsion rheology and oil recovery [33, 4] to relatively recent bioimaging and efficient drug delivery [7, 46]. Taylor [33, 34] was arguably the first to offer a systematic analysis of this problem, and since then there have been numerous theoretical and experimental studies that considered the drop and the ambient fluid under various conditions including but not limited to the presence of either externally imposed linear flow or an electric field or a combination of both. For a comprehensive review of this subject, see, e.g., [24, 31, 19, 27, 17], to mention just a few.

This work focuses on the drop deformation problem under arbitrary axisymmetric boundary conditions linearized with respect to the velocity field. Particular cases of this problem are those when the drop is embedded into extensional/compressional flow [4, 1, 25, 32, 50, 51], when the drop and the ambient flow are under the presence of a uniform electric field with at least one of them being nonconducting [3, 36, 26, 20] or both being slightly conducting (so-called leaky dielectrics) [37, 2, 29, 40, 38, 14, 9, 6, 17, 48], and when they are subjected to aligned extensional/compressional flow

*Received by the editors November 16, 2015; accepted for publication (in revised form) May 27, 2016; published electronically August 18, 2016.
http://www.siam.org/journals/siap/76-4/M104847.html
†Department of Mathematical Sciences, Stevens Institute of Technology, Castle Point on Hudson, Hoboken, NJ 07030 (mzabaran@stevens.edu).

and a uniform electric field provided that surface charge convection is negligible. The key parameters in these cases are capillary number Ca and electric capillary number Ca_E that characterize the balance of the strength of the linear flow and of the electric field to the drop surface tension, respectively:[1] for $\mathrm{Ca} = 0$ and $\mathrm{Ca}_E = 0$, an initially spherical drop remains undeformed, and when only either linear flow or an electric field is applied, an increase in Ca or Ca_E yields larger deformations.

The methods for solving the drop deformation problem are divided into two major classes: small deformation theories and large deformation theories. The first class is represented by first-order [37, 8, 13, 23, 18], second-order [4, 2, 22], and recent third-order [43] approximations in Ca and Ca_E, which assume the shape of the drop to be nearly spherical and expand the velocity field in terms of spherical harmonics, whereas the second one includes the slender body theory [35, 1, 47] and numerical techniques such as finite element methods (FEMs) [5, 10] and boundary integral equations (BIEs) [25, 29, 17]. While the first-order and second-order approximations agree with the experimental results [14] for the Taylor deformation parameter D up to 0.02 and 0.1, respectively, FEMs and BIEs, particularly when Ca or Ca_E is close to its critical value, are computationally expensive. Yet, since Allan and Mason [3] and Taylor [36], theoretical and experimental studies have indicated that under various conditions the deformed drop, being initially spherical, has the steady shape close to prolate/oblate spheroidal even for nonsmall D, and the spheroidal drop approximation was used for drop deformation analysis when at least one of the phases is dielectric [36, 26, 20], when both phases are leaky dielectrics [6, 48, 54, 22], and when the drop is embedded in a linear flow [45, 44, 50, 51, 21]. For example, in the case of an extensional (compressional) flow, the steady shape is close to prolate (oblate) spheroidal for D up to 0.3 [50, 51], whereas under the presence of a uniform electric field a leaky dielectric drop can remain approximately prolate/oblate spheroidal for $|D| \sim 0.4$ [17, 48]. It is shown in [50, 48] that predictions for critical Ca and critical Ca_E based on analytical solutions for spheroidal drops are much closer to those that follow from the BIE approach than to those implied by the second-order approximation theory. Thus, the spheroidal drop approach bridges the gap between the small and large deformation theories and can be a valuable alternative to the BIE approach due to its computational efficiency and capability of providing analytical insights into the analysis of various characteristics.

In general, a spheroidal drop of fixed volume is not at steady state since with a single free parameter, e.g., axes ratio, it cannot satisfy the governing equations and velocity and stress boundary conditions along with a kinematic condition exactly. Which equations and conditions to satisfy exactly and which just approximately is a matter of tradeoff between computational simplicity and accuracy of deformation prediction. For example, the extended leaky dielectric model (ELDM) [6], being relatively simple, does not satisfy the Stokes equations inside a spheroidal drop and matches the tangential and normal stress boundary conditions approximately.[2] How-

[1] $\mathrm{Ca} = \mu^- G l/\gamma$ and $\mathrm{Ca}_E = \varepsilon_0 \varepsilon^- E_\infty^2 l/\gamma$, where μ^- and ϵ^- are the viscosity and dielectric constant of the ambient fluid, respectively, G is the share rate of the linear flow, l is the radius of an initially spherical drop, γ is the surface tension coefficient, E_∞ is the strength of the electric field, and ϵ_0 is the vacuum permittivity.

[2] Zhang, Zahn, and Lin [54] and Nganguia et al. [22] used ELDM stream functions [6] to approximate the velocity fields in an ambient fluid and in a spheroidal drop subject to a uniform electric field, whereas Narsimhan, Spann, and Shaqfeh [21, Appendix A.4] found analytically the velocity field of a viscous flow with a spheroidal vesicle that satisfied only velocity boundary conditions as those for a rigid particle.

ever, it shows a good agreement with the experimental results in [6] and with some experimental data from [14]. In fact, a drop of arbitrary fixed shape can satisfy exactly all the governing equations and conditions but one, so that one condition can be excluded and used for finding a steady shape. For this purpose, several studies, which assume a specific drop's shape, e.g., a spindle-shaped drop in an extensional flow [28] and two liquid equal spheres in a conducting fluid under the presence of an electric field [30], choose the normal stress boundary condition. In contrast, the BIE approach [25] and the closely related drop dynamics simulation satisfy the governing equations and all velocity and stress boundary conditions and then use the kinematic condition to update the drop shape. In any case, finding a steady shape is a computationally expensive iterative procedure. Moreover, the steady shape depends on the capillary number, so in order to find dependence of D on either Ca or Ca_E (deformation curve), the procedure should be repeated for a range of capillary numbers. For a family of shapes parametrized by one or two free parameters, e.g., spheroids, spindles, etc., deformation curves can, in fact, be efficiently found from the inverse problem [48], which for each shape minimizes the square error of the kinematic condition with respect to Ca (or Ca_E).[3] The inverse problem takes advantage of the fact that the velocity field linearly depends on $1/\mathrm{Ca}$ (or $1/\mathrm{Ca}_E$), which implies that the kinematic condition error is a quadratic function of $1/\mathrm{Ca}$ (or $1/\mathrm{Ca}_E$) and, thus, its minimizer has a simple analytical form. Although the deformation curves obtained from the inverse problem are not identical to those found from the direct problem that minimizes the kinematic condition error with respect to shape parameter for given Ca (or Ca_E), Zabarankin [48] showed that for a leaky dielectric spheroidal drop they match the deformation curves for the BIE-based steady shapes from [17] remarkably well up to critical values of Ca_E (generally for $|D| \leqslant 0.4$).

This work is motivated by two reasons. The first is to study nonsmall deformations for a drop in aligned linear flow and a uniform electric field under the assumptions that the phases are leaky dielectrics and that surface charge convection is negligible. There are only a few studies dedicated to the analysis of drop dynamics due to the cumulative effect of imposed flow and electric field [3, 15, 12, 11, 41], and almost all of them deal with small deformations and pure shear flow, whereas understanding the interplay between electric and flow fields is critical for harnessing flow control in various biomedical applications [42, 46]. The second reason is rather technical. In [50, 51, 48], the approach of generalized analytic functions reduced the velocity and stress boundary conditions to a first-order difference equation for coefficients in infinite series representing the velocity field. The solution of the equation was given by a recursion and involved an unknown constant, whose determination required the knowledge of all terms in the recursion. This work shows that the stress boundary conditions can be reformulated in a way suitable for a relatively straightforward application of a stream function approach that yields an exact nonrecursive analytical solution satisfying exactly not only the Stokes equations inside and outside a spheroidal drop and the velocity boundary conditions but also arbitrary axisymmetric linearized stress boundary conditions. In the case of extensional/compressional flow, the deformation curves and critical Ca for "steady" spheroids are close to those predicted by the BIE approach [25, 24, 51], whereas under the presence of only the electric field, the deformation curves, obtained here and in [48], do not generally coincide but match those for the BIE-based steady shapes [17] equally well.

[3] The direct problem finds a stationary shape for given strengths of external flow/electric fields, whereas the inverse problem finds strengths of the external fields to make a given shape stationary.

The organization and contribution of this work are as follows. Section 2 formulates the problem of a liquid drop embedded in another fluid under the presence of aligned external linear flow and a uniform electric field. It also reformulates the stress boundary conditions and constructs a stream function-solution form. Section 3 tests the suggested solution form for a spherical drop and finds conditions under which the drop either remains spherical or is either prolate or oblate. Section 4 solves the problem for a spheroidal drop and identifies conditions for "steady" spheroids. Section 5 evaluates "steady" spheroid deformations as a function of Ca and Ca_E for various ratios of drop/ambient fluid characteristics. Section 6 concludes the work. The supplementary materials contain details of some derivations and additional numerical results.

2. Problem formulation. Suppose a liquid drop of volume $4\pi\, l^3/3$ is embedded into an unbounded fluid, and suppose the drop and the ambient fluid occupy regions $\mathbb{D}^+$ and $\mathbb{D}^-$, respectively, with common boundary S, so that $\mathbb{D}^+ \cup \mathbb{D}^- = \mathbb{R}^3$. The liquids in $\mathbb{D}^\pm$ are both considered to be viscous and incompressible with corresponding viscosities $\mu^\pm$. Without the drop, the fluid occupying $\mathbb{R}^3$ is subject to a linear axisymmetric flow $\mathbf{u}^\infty = G(-x\,\mathbf{i} - y\,\mathbf{j} + 2z\,\mathbf{k})$, where (x, y, z) is the Cartesian coordinate system with the basis $(\mathbf{i}, \mathbf{j}, \mathbf{k})$ and G is the shear rate with $G > 0$ and $G < 0$ corresponding to extensional and compressional flows, respectively. The drop and the fluid are assumed to be leaky dielectrics with corresponding dielectric constants $\varepsilon^\pm$ and electric conductivities $\sigma^\pm$ and are also assumed to be under the presence of a uniform electric field $\mathbf{E}^\infty = E_\infty\,\mathbf{k}$. Let $\lambda = \mu^+/\mu^-$, $R = \sigma^-/\sigma^+$, and $Q = \varepsilon^+/\varepsilon^-$.

In the absence of a magnetic field and electric charges inside and outside the drop, the stationary electric field $\mathbf{E}^\pm$ in $\mathbb{D}^\pm$ is irrotational and divergence-free:

$$\operatorname{curl}\mathbf{E}^\pm = 0, \qquad \operatorname{div}\mathbf{E}^\pm = 0 \qquad \text{in} \quad \mathbb{D}^\pm, \tag{1}$$

and $\mathbf{E}^-$ approaches $\mathbf{E}^\infty$ at infinity. Let $E_n^\pm = \mathfrak{n}\cdot\mathbf{E}^\pm$, where $\mathfrak{n}$ is the outward normal for the surface S. Then the tangential component $\mathbf{E}_t^\pm = \mathbf{E}^\pm - E_n^\pm\mathfrak{n}$ is continuous across S, and under the assumption of $|G\varepsilon^-/\sigma^-| \ll 1$, which implies that surface charge convection coupling the flow and electric fields is negligible, the normal component $E_n^\pm$ satisfies $\sigma^+ E_n^+ = \sigma^- E_n^-$ on S; see, e.g., [41, eq. (2.18)]. Thus, the boundary conditions for $\mathbf{E}^\pm$ are given by

$$\sigma^+ E_n^+\big|_S = \sigma^- E_n^-\big|_S\,, \qquad \mathbf{E}_t^+\big|_S = \mathbf{E}_t^-\big|_S\,, \qquad \mathbf{E}^-\big|_\infty = \mathbf{E}^\infty. \tag{2}$$

The induced surface charge density on S is determined by $\varepsilon_0\,(\varepsilon^- E_n^- - \varepsilon^+ E_n^+)$, where ε_0 is the vacuum permittivity.

Let $p^\pm$ and $\mathbf{u}^\pm$ be the pressure and the velocity disturbance in $\mathbb{D}^\pm$, respectively ($\mathbf{u}^\infty + \mathbf{u}^\pm$ is the velocity field in $\mathbb{D}^\pm$). Under the assumption of negligible inertial, gravitational, and thermal effects, the steady-state fluid flow in $\mathbb{D}^\pm$ is governed by the Stokes (creeping flow) equations

$$\mu^\pm\,\boldsymbol{\Delta}\mathbf{u}^\pm = \operatorname{grad} p^\pm, \qquad \operatorname{div}\mathbf{u}^\pm = 0 \qquad \text{in} \quad \mathbb{D}^\pm, \tag{3}$$

with $\boldsymbol{\Delta}\mathbf{u} \equiv \operatorname{grad}\operatorname{div}\mathbf{u} - \operatorname{curl}\operatorname{curl}\mathbf{u}$. The velocity disturbance $\mathbf{u}^\pm$ is continuous across the surface S and, along with the pressure, it vanishes at infinity:

$$\mathbf{u}^-\big|_S = \mathbf{u}^+\big|_S\,, \qquad \mathbf{u}^-\big|_\infty = 0, \qquad p^-\big|_\infty = 0. \tag{4}$$

A force balance across the interface yields the boundary conditions for the stress

$$\mathbf{P}_n^+\big|_S - \mathbf{P}_n^-\big|_S = \mathbf{F}, \tag{5}$$

where the stress vectors $\mathbf{P}_n^{\pm}$ are determined by

$$\mathbf{P}_n^{\pm} = -p^{\pm}\,\mathfrak{n} + 2\mu^{\pm}\frac{\partial}{\partial n}\left(\mathbf{u}^{\pm}+\mathbf{u}^{\infty}\right) + \mu^{\pm}\left[\mathfrak{n}\times\operatorname{curl}\mathbf{u}^{\pm}\right], \tag{6}$$

and $\mathbf{F}$ includes the interfacial tension $\mathbf{F}_\gamma = -\gamma\,\mathfrak{n}\operatorname{div}\mathfrak{n}$, with γ being a constant and $\operatorname{div}\mathfrak{n}$ the surface curvature, and the interfacial jump $\mathbf{F}_E = (\mathcal{T}^- - \mathcal{T}^+)\mathfrak{n}$ of the Maxwell stress tensors $\mathcal{T}_{ij}^{\pm} = \varepsilon_0\,\varepsilon^{\pm}\,(E_i^{\pm}\,E_j^{\pm} - \delta_{ij}\,E_k^{\pm}\,E_k^{\pm}/2)$ due to the electric field, so that

$$\mathbf{F} = \underbrace{-\gamma\,\mathfrak{n}\operatorname{div}\mathfrak{n}}_{=\mathbf{F}_\gamma} + \underbrace{\frac{\varepsilon_0\,\varepsilon^-}{2}\left(\left[(1-QR^2)(E_n^-)^2 - (1-Q)(E_t^-)^2\right]\mathfrak{n} + 2(1-RQ)E_n^-\,\mathbf{E}_t^-\right)}_{=\mathbf{F}_E}, \tag{7}$$

where $(E_t^-)^2 = \mathbf{E}_t^-\cdot\mathbf{E}_t^-$; see [17, 48] for details.

The drop is at steady state when the interface has zero normal velocity, i.e.,

$$\left(\mathbf{u}^{\pm}+\mathbf{u}^{\infty}\right)\cdot\mathfrak{n} = 0 \quad \text{on} \quad S, \tag{8}$$

which is called the kinematic condition.

Let (r,φ,z) be the system of cylindrical coordinates with the basis $(\mathbf{e}_r,\mathbf{e}_\varphi,\mathbf{e}_z)$ and related to the Cartesian coordinates in the ordinary way; then

$$\mathbf{u}^{\infty} = u_r^{\infty}\mathbf{e}_r + u_z^{\infty}\mathbf{e}_z = G\,(-r\,\mathbf{e}_r + 2z\,\mathbf{e}_z), \qquad \mathbf{E}^{\infty} = E_\infty\,\mathbf{e}_z. \tag{9}$$

Suppose the drop has the axis of revolution coinciding with the z-axis and is centered at the origin. In this case, problem (3)–(9) is axially symmetric, i.e., $\mathbf{u}^{\pm}$ and $p^{\pm}$ are independent of the angular coordinate φ:

$$\mathbf{u}^{\pm}(r,\varphi,z) = u_r^{\pm}(r,z)\,\mathbf{e}_r + u_z^{\pm}(r,z)\,\mathbf{e}_z, \qquad \operatorname{curl}\mathbf{u}^{\pm} = \omega^{\pm}(r,z)\,\mathbf{e}_\varphi, \qquad p^{\pm} = p^{\pm}(r,z),$$

where the scalar vorticity functions $\omega^{\pm}$ are defined by

$$\omega^{\pm} = \frac{\partial u_r^{\pm}}{\partial z} - \frac{\partial u_z^{\pm}}{\partial r}, \tag{10}$$

and $\operatorname{div}\mathbf{u}^{\pm} = 0$ takes the form

$$\frac{\partial u_r^{\pm}}{\partial r} + \frac{u_r^{\pm}}{r} + \frac{\partial u_z^{\pm}}{\partial z} = 0. \tag{11}$$

Further, $\mathbf{F}$ is assumed to be an arbitrary axisymmetric vector: $\mathbf{F} = F_r(r,z)\,\mathbf{e}_r + F_z(r,z)\,\mathbf{e}_z$, and (7) is treated as a particular case—this is the reason why the velocity, stress, and electric fields are not dimensionalized at this stage.

2.1. Reformulation of the stress boundary conditions. Let ℓ be the cross section of the drop surface S in the rz-half plane. On ℓ, the normal vector $\mathfrak{n}$ is directed outward, and the tangential vector $\mathfrak{s}$ is aligned with the counterclockwise orientation of ℓ. In this case,

$$\mathfrak{n} = \frac{\partial r}{\partial n}\,\mathbf{e}_r + \frac{\partial z}{\partial n}\,\mathbf{e}_z, \qquad \mathfrak{s} = [\mathfrak{n}\times\mathbf{e}_\varphi] = \frac{\partial r}{\partial s}\,\mathbf{e}_r + \frac{\partial z}{\partial s}\,\mathbf{e}_z,$$

where $\partial/\partial n$ and $\partial/\partial s$ are normal and tangential derivatives, respectively, and

$$\frac{\partial r}{\partial s} = -\frac{\partial z}{\partial n}, \qquad \frac{\partial r}{\partial n} = \frac{\partial z}{\partial s}. \tag{12}$$

With (12), the expressions (10) $\frac{\partial r}{\partial s}$ − (11) $\frac{\partial z}{\partial s}$ and (10) $\frac{\partial z}{\partial s}$ + (11) $\frac{\partial r}{\partial s}$ yield

$$\omega^{\pm}\frac{\partial r}{\partial s} = -\frac{\partial u_r^{\pm}}{\partial n} - \frac{u_r^{\pm}}{r}\frac{\partial z}{\partial s} - \frac{\partial u_z^{\pm}}{\partial s}, \qquad \omega^{\pm}\frac{\partial z}{\partial s} = -\frac{\partial u_z^{\pm}}{\partial n} + \frac{u_r^{\pm}}{r}\frac{\partial r}{\partial s} + \frac{\partial u_r^{\pm}}{\partial s},$$

and the sum of the latter multiplied by $\mathbf{e}_r$ and $\mathbf{e}_z$, respectively, results in

$$\frac{\partial \mathbf{u}^{\pm}}{\partial n} = -\omega^{\pm}\mathfrak{s} - \frac{\partial u_z^{\pm}}{\partial s}\mathbf{e}_r + \frac{\partial u_r^{\pm}}{\partial s}\mathbf{e}_z - \frac{u_r^{\pm}}{r}\,\mathfrak{n}. \tag{13}$$

Then the relationship (13) implies that

$$\mathbf{P}_n^{\pm} = -p^{\pm}\,\mathfrak{n} - \mu^{\pm}\omega^{\pm}\,\mathfrak{s} - 2\mu^{\pm}\left(\frac{\partial(u_z^{\pm}+u_z^{\infty})}{\partial s}\mathbf{e}_r - \frac{\partial(u_r^{\pm}+u_r^{\infty})}{\partial s}\mathbf{e}_z + \frac{u_r^{\pm}+u_r^{\infty}}{r}\,\mathfrak{n}\right), \tag{14}$$

which being projected onto $\mathbf{e}_z$ and multiplied by r yields

$$r\,\mathbf{P}_n^{\pm}\cdot\mathbf{e}_z = r\left(p^{\pm}\,\frac{\partial r}{\partial s} - \mu^{\pm}\omega^{\pm}\,\frac{\partial z}{\partial s}\right) + 2\mu^{\pm}\frac{\partial\,(r(u_r^{\pm}+u_r^{\infty}))}{\partial s}. \tag{15}$$

Since the pressure $p^{\pm}$ and vorticity $\omega^{\pm}$ are related by the Stokes–Beltrami equations

$$\frac{\partial p^{\pm}}{\partial r} = \mu^{\pm}\frac{\partial \omega^{\pm}}{\partial z}, \qquad \frac{\partial p^{\pm}}{\partial z} = -\frac{\mu^{\pm}}{r}\frac{\partial}{\partial r}(r\,\omega^{\pm}),$$

they can be represented in terms of 1-harmonic functions $\Phi^{\pm}$ as

$$p^{\pm} = -\frac{2\mu^{\pm}}{r}\,\frac{\partial}{\partial r}(r\,\Phi^{\pm}) + C^{\pm}, \qquad \omega^{\pm} = 2\,\frac{\partial \Phi^{\pm}}{\partial z}, \qquad \Delta_1\Phi^{\pm} = 0, \tag{16}$$

where $C^- = 0$, C^+ is an arbitrary constant, and Δ_k is the k-harmonic operator:

$$\Delta_k \equiv \frac{\partial^2}{\partial r^2} + \frac{1}{r}\frac{\partial}{\partial r} + \frac{\partial^2}{\partial z^2} - \frac{k^2}{r^2}.$$

With the representation (16), the expression (15) takes the form

$$r\,\mathbf{P}_n^{\pm}\cdot\mathbf{e}_z = 2\mu^{\pm}\frac{\partial}{\partial s}\left(r\,(u_r^{\pm}+u_r^{\infty}-\Phi^{\pm})\right) + C^{\pm}\,r\,\frac{\partial r}{\partial s}.$$

Projecting the stress boundary condition (5) onto $\mathbf{e}_z$, multiplying the projection by r, and integrating it with respect to the curve length s, i.e., $\int r\,(5)\cdot\mathbf{e}_z\,ds$, we obtain

$$\left[\mu^*\,(u_r^*+u_r^{\infty}-\Phi^*) + \frac{C^*}{4}r\right]\Bigg|_-^+ = \underbrace{\frac{1}{2r}\int r\,F_z\,ds}_{=F_1} \quad \text{on} \quad \ell, \tag{17}$$

where $[(\cdot)^*]|_-^+ = (\cdot)^+ - (\cdot)^-$ denotes the jump over the interface, and the constant of integration in F_1 is chosen such that F_1 vanishes as $r \to 0$ if the z-axis goes through the drop (this may not be necessary if the drop has a toroidal shape).

Similarly, with (14), the combination $\frac{1}{2}(5)\cdot\mathbf{e}_r + \frac{1}{r}\frac{\partial r}{\partial n}(17)$ yields

$$\left[\mu^*\left(\frac{\partial\Phi^*}{\partial n} - \frac{\partial(u_z^*+u_z^{\infty})}{\partial s}\right) - \frac{C^*}{4}\frac{\partial r}{\partial n}\right]\Bigg|_-^+ = \frac{1}{2}F_r + \frac{1}{r}\frac{\partial r}{\partial n}F_1 \quad \text{on} \quad \ell,$$

which being integrated with respect to the curve length s results in

$$\left[\mu^*\left(\widetilde{\Phi}^* - u_z^* - u_z^\infty\right) - \frac{C^*}{4}z\right]\Big|_-^+ = \underbrace{\int\left(\frac{1}{2}F_r + \frac{1}{r}\frac{\partial r}{\partial n}F_1\right)ds}_{=F_2} \quad \text{on} \quad \ell, \tag{18}$$

where

$$\widetilde{\Phi}^\pm = \int \frac{\partial \Phi^\pm}{\partial n}\,ds \quad \text{on} \quad \ell. \tag{19}$$

Thus, in the axially symmetric case with the z-axis being the axis of revolution, the stress boundary conditions (5) can be reformulated as the system (17)–(19). Observe that F_1 and F_2 contain arbitrary constants of integration.

As a particular case, consider $\mathbf{F} = \mathbf{F}_\gamma \equiv -\gamma\,\mathfrak{n}\,\mathrm{div}\,\mathfrak{n}$. Let ℓ be parametrized in terms of its length s, which increases in the counterclockwise direction of ℓ: $r = r(s)$ and $z = z(s)$; then

$$\mathrm{div}\,\mathfrak{n} = r'_s\,z''_{ss} - r''_{ss}\,z'_s + z'_s/r \quad \text{on} \quad \ell,$$

where $(\cdot)'_s$ denotes the derivative with respect to s. The identity $(r'_s)^2 + (z'_s)^2 \equiv 1$ implies that $r''_{ss}\,r'_s + z''_{ss}\,z'_s \equiv 0$, whence $r''_s = -z''_{ss}\,z'_s/r'_s$, and consequently

$$\mathrm{div}\,\mathfrak{n} = r'_s\,z''_{ss} + \frac{z''_{ss}}{r'_s}\,(z'_s)^2 + \frac{z'_s}{r} = \frac{z''_{ss}}{r'_s} + \frac{z'_s}{r} = \frac{(r\,z'_s)'_s}{r\,r'_s} \quad \text{on} \quad \ell.$$

Then with the relationships (12) we obtain

$$\begin{aligned} F_1 &= \frac{\gamma}{2}\,z'_s + \widetilde{C}_1, \\ F_2 &= \frac{\gamma}{2}\int\left(r''_{ss}\,z'_s - r'_s\,z''_{ss}\right)z'_s\,ds = \frac{\gamma}{2}\int\left(r''_{ss}\,(r'_s)^2 + r''_{ss}\,(z'_s)^2\right)ds = \frac{\gamma}{2}\,r'_s + \widetilde{C}_2, \end{aligned} \tag{20}$$

where $\widetilde{C}_1$ and $\widetilde{C}_2$ are constants of integration to be put to zero.

2.2. Non-Stokes stream function. In the axially symmetric case with the z-axis of revolution, the velocity field $\mathbf{u}^\infty$ and its disturbance $\mathbf{u}^\pm$ can be represented in terms of *non-Stokes bi-1-harmonic* stream functions $\Psi^\infty = -G\,r\,z$ and $\Psi^\pm = \Psi^\pm(r,z)$, respectively, as in [39, eq. (42.1)]:[4]

$$\mathbf{u}^* = -\,\mathrm{curl}(\Psi^*\,\mathbf{e}_\varphi), \qquad \Delta_1^2\Psi^* = 0, \tag{21}$$

where "$*$" stands for "∞," "$+$," and "$-$." The representation (21) was used in hydrodynamics problems on the motion of axially symmetric solid particles in a viscous incompressible fluid; see [52, 53, 49]. In component form, it is given by

$$u_r^* = \frac{\partial\Psi^*}{\partial z}, \qquad u_\varphi^* \equiv 0, \qquad u_z^* = -\frac{1}{r}\frac{\partial}{\partial r}(r\,\Psi^*). \tag{22}$$

The velocity boundary conditions (4) imply that

$$\Psi^+ - \Psi^- = \frac{C_\psi}{r}, \qquad \frac{\partial\Psi^+}{\partial n} - \frac{\partial\Psi^-}{\partial n} = -\frac{C_\psi}{r^2}\frac{\partial r}{\partial n} \quad \text{on} \quad \ell, \qquad \Psi^-\big|_\infty = 0, \tag{23}$$

[4] $\Psi^\pm$ are related to Stokes stream functions $\Psi_S^\pm$ by $\Psi_S^\pm = -r\,\Psi^\pm$. While the former are bi-1-harmonic functions, the latter satisfy $E^4\Psi_S^\pm = 0$ with $E^2 = \partial^2/\partial r^2 - r^{-1}\partial/\partial r + \partial^2/\partial z^2$; see [16].

where C_ψ is a constant of integration, which is zero since $\Psi^\pm$ and Ψ^∞ are odd functions of z. (If the z-axis goes through the drop, then $C_\psi = 0$ regardless of whether $\Psi^\pm$ and Ψ^∞ are odd or even functions of z.) Similarly, $r\,(\Psi^+ + \Psi^\infty)$, being an odd function of z, cannot be a nonzero constant on ℓ, and the kinematic condition (8) yields

$$\Psi^+ + \Psi^\infty = 0 \quad \text{on} \quad \ell. \tag{24}$$

Further, $\Psi^\pm$ can be represented in terms of the 1-harmonic functions $\Phi^\pm$ introduced in (16) and of 1-harmonic functions $\Omega^\pm$ by [39, eq. (42.2)]

$$\Psi^\pm = z\,\Phi^\pm + \Omega^\pm, \qquad \Delta_1 \Omega^\pm = 0, \tag{25}$$

and the pressure $p^\pm$ and vorticity $\omega^\pm = \Delta_1 \Psi^\pm$ are determined by (16).

The terms with the constant C^+ in (17)–(18) can be satisfied by the functions $\Phi^+ = C^+ r/(4\mu^+)$ and $\Omega^+ = -C^+ r\,z/(4\mu^+)$, which collectively make no contribution to Ψ^+ and will further be omitted.

The combinations (17) $\frac{\partial z}{\partial s}$ + (18) $\frac{\partial r}{\partial s}$ and (17) $\frac{\partial z}{\partial n}$ + (18) $\frac{\partial r}{\partial n}$ yield

$$\begin{aligned}
&\left[\mu^* \left(\frac{1}{r}\frac{\partial}{\partial s}(r(\Psi^* + \Psi^\infty)) + \widetilde{\Phi}^* \frac{\partial r}{\partial s} - \Phi^* \frac{\partial z}{\partial s}\right)\right]\Bigg|_-^+ = F_1 \frac{\partial z}{\partial s} + F_2 \frac{\partial r}{\partial s} \quad \text{on} \quad \ell,\\
&\left[\mu^* \left(\frac{1}{r}\frac{\partial}{\partial n}(r(\Psi^* + \Psi^\infty)) + \widetilde{\Phi}^* \frac{\partial r}{\partial n} - \Phi^* \frac{\partial z}{\partial n}\right)\right]\Bigg|_-^+ = F_1 \frac{\partial z}{\partial n} + F_2 \frac{\partial r}{\partial n} \quad \text{on} \quad \ell,
\end{aligned} \tag{26}$$

where F_1 and F_2 are defined in (17) and (18), respectively, in particular,

$$\text{for} \quad \mathbf{F} = \mathbf{F}_\gamma \equiv -\gamma\,\mathfrak{n}\,\mathrm{div}\,\mathfrak{n}, \qquad F_1 \frac{\partial z}{\partial s} + F_2 \frac{\partial r}{\partial s} = \frac{\gamma}{2}, \qquad F_1 \frac{\partial z}{\partial n} + F_2 \frac{\partial r}{\partial n} = 0.$$

Thus, the stream functions $\Psi^\pm$ represented by (25) and the functions $\widetilde{\Phi}^\pm$ defined by (19) should satisfy the boundary conditions (23) and (26) with $C_\psi = 0$.

When the drop's and ambient fluid's viscosities are equal, i.e., $\mu^+ = \mu^- = \mu$, the boundary conditions (23) and (26) with $C_\psi = 0$ simplify to

$$\begin{aligned}
&[\Phi^*]\big|_-^+ = -\frac{F_1}{\mu}, \qquad \left[\frac{\partial \Phi^*}{\partial n}\right]\Bigg|_-^+ = \frac{F_r}{2\mu} + \frac{z'_s F_1}{\mu r} \quad \text{on} \quad \ell,\\
&[\Omega^*]\big|_-^+ = \frac{z\,F_1}{\mu}, \qquad \left[\frac{\partial \Omega^*}{\partial n}\right]\Bigg|_-^+ = -\frac{z\,F_r}{2\mu} - \frac{r r'_s + z z'_s}{\mu r} F_1 \quad \text{on} \quad \ell,
\end{aligned} \tag{27}$$

which allow finding $\Phi^\pm$ and $\Omega^\pm$, and consequently $\Psi^\pm$, in a closed (integral) form for any ℓ through the fundamental solution for 1-harmonic functions. In fact, a closed-form solution for $\mathbf{u}^\pm$ in this case is well known; see, e.g., [25, 50].

For $\mathbf{F} = \mathbf{F}_\gamma \equiv -\gamma\,\mathfrak{n}\,\mathrm{div}\,\mathfrak{n}$, the boundary conditions (27) are particularly simple:

$$[\Phi^*]\big|_-^+ = -\frac{\gamma\,z'_s}{2\mu}, \quad \left[\frac{\partial \Phi^*}{\partial n}\right]\Bigg|_-^+ = \frac{\gamma\,r''_{ss}}{2\mu}, \quad [\Omega^*]\big|_-^+ = \frac{\gamma\,z\,z'_s}{2\mu}, \quad \left[\frac{\partial \Omega^*}{\partial n}\right]\Bigg|_-^+ = -\frac{\gamma\,(r'_s\,z)'_s}{2\mu}.$$

3. Spherical drop. This section solves problem (1)–(7) with (9) for a spherical drop being embedded into the linear flow $\mathbf{u}^\infty$ and subjected to the uniform electric field $\mathbf{E}^\infty$. Its aim is to determine when the drop remains spherical, deforms into a prolate spheroid, and deforms into an oblate spheroid. See *section* S1 *in the supplementary materials* for the full version of this section.

Let spherical coordinates (ρ,ϑ,φ), with $\rho\geqslant 0$, $\vartheta\in[0,\pi]$, and $\varphi\in[0,2\pi]$, be related to the cylindrical coordinates in the ordinary way: $r=\rho\sin\vartheta$ and $z=\rho\cos\vartheta$, and let the spherical drop of radius l be centered at the origin. Then

$$\Psi^\infty=-G\,r\,z=\frac{G}{3}\rho^2\,\mathrm{P}_2^{(1)}(\cos\vartheta),$$

where $\mathrm{P}_n^{(k)}(\cos\vartheta)$ is the associated Legendre polynomial of the first kind of order n and rank k (for $k=0$, the superscript is omitted). In this case, $\operatorname{div}\mathfrak{n}=2/l$,

$$E_n^-\big|_{\rho=l}=\frac{3E_\infty\cos\vartheta}{1+2R},\qquad E_t^-\big|_{\rho=l}=\frac{3E_\infty R\sin\vartheta}{1+2R},\qquad \vartheta\in[0,\pi],$$

$$F_1=\frac{\gamma}{2}\sin\vartheta+\frac{9\varkappa l}{16(1+2R)^2}\left(2\left(QR^2-1\right)\sin\vartheta+(R-1)^2\sin^3\vartheta\right),$$
$$F_2=-\frac{\gamma}{2}\cos\vartheta+\frac{9\varkappa l}{16(1+2R)^2}\left(\left(2R^2(3Q-1)-(R+1)^2\right)\cos\vartheta+(R-1)^2\cos^3\vartheta\right),$$

with $\varkappa=\varepsilon_0\varepsilon^-E_\infty^2$, and

$$\Psi^+=\left(\left(\frac{1}{3}A_1^+ + B_2^+\right)\rho^2+\frac{4}{7}A_3^+\rho^4\right)\mathrm{P}_2^{(1)}(\cos\vartheta),\qquad \vartheta\in[0,\pi],$$
$$\Psi^-=\left(\frac{1}{3}A_1^-\rho^{-1}+B_2^-\rho^{-3}\right)\mathrm{P}_2^{(1)}(\cos\vartheta),\qquad \vartheta\in[0,\pi]$$

(see *equation* (S1) *in the supplementary materials*), where $A_1^\pm$, A_3^+, and $B_2^\pm$ are found from the boundary conditions (23) and (26):

$$A_1^+=\frac{\gamma}{2l\mu^+}+3\varkappa\frac{2R(1-QR)(19\lambda+16)+(R-1)^2(16\lambda+19)}{2\mu^-(1+2R)^2(2\lambda+3)(19\lambda+16)},$$
$$A_3^+=-\frac{21\varkappa\,(R-1)^2}{8\mu^-l^2(1+2R)^2(19\lambda+16)},\qquad B_2^+=-\frac{\gamma}{6l\mu^+}+\frac{2G(1-\lambda)}{3(2\lambda+3)},$$
$$A_1^-=\frac{5G(1-\lambda)\,l^3}{2\lambda+3}+3\varkappa l^3\,\frac{1+3R+R^2(1-5Q)}{2\mu^-(1+2R)^2(2\lambda+3)},$$
$$B_2^-=\frac{G(\lambda-1)\,l}{2\lambda+3}-3\varkappa l^5\,\frac{R(1-QR)(19\lambda+16)+(R-1)^2(3\lambda+2)}{2\mu^-(1+2R)^2(2\lambda+3)(19\lambda+16)}.$$

On the boundary, the normal velocity $(\mathbf{u}^+ + \mathbf{u}^\infty)\cdot\mathfrak{n}\equiv u_n^+ + u_n^\infty$ takes the form

$$(u_n^+ + u_n^\infty)\big|_{\rho=l}=\left[\frac{1}{r}\frac{\partial}{\partial s}(r(\Psi^+ + \Psi^\infty))\right]\Big|_{\rho=l}=\frac{6\varkappa l\,\mathfrak{D}}{\mu^-(2\lambda+3)}\,\mathrm{P}_2(\cos\vartheta),$$

where

$$\mathfrak{D}=\frac{R(1-QR)}{(1+2R)^2}+\frac{5(R-1)^2(\lambda+1)}{(1+2R)^2(19\lambda+16)}+\frac{5\,\mathrm{Ca}}{3\,\mathrm{Ca}_E},\tag{28}$$

with $\mathrm{Ca}=\mu^-Gl/\gamma$ and $\mathrm{Ca}_E=\varkappa l/\gamma$ being the capillary number and electric capillary number, respectively. The quotient $\mathrm{Ca}_E/\mathrm{Ca}$ is known as the Mason parameter Mn.

When $\mathfrak{D}=0$, $(u_n^+ + u_n^\infty)|_{\rho=l}\equiv 0$, and the drop remains spherical, whereas when $\mathfrak{D}>0$ ($\mathfrak{D}<0$), the north pole of the drop has positive (negative) normal velocity,

which indicates that the drop is going to elongate (compress). Thus, the drop becomes prolate/oblate when $\mathfrak{D} \gtrless 0$. Let

$$\widetilde{\mathscr{F}}(R,Q,\lambda) = \frac{3(RQ-1)R}{5(1+2R)^2} - \frac{3(\lambda+1)}{19\lambda+16}\frac{(R-1)^2}{(1+2R)^2} \equiv -\frac{3(\lambda+1)\,\mathscr{F}(R,Q,\lambda)}{(19\lambda+16)(1+2R)^2}, \tag{29}$$

where

$$\mathscr{F}(R,Q,\lambda) = (R-1)^2 + R(1-QR)\frac{19\lambda+16}{5(1+\lambda)} \tag{30}$$

is the Taylor discriminating function [37]. Then $\mathfrak{D} = 5(\mathrm{Ca}/\mathrm{Ca}_E - \widetilde{\mathscr{F}}(R,Q,\lambda))/3$, and the conditions for the drop to remain *spherical* or to become *prolate/oblate* are given by

$$\mathrm{Ca} = \mathrm{Ca}_E\,\widetilde{\mathscr{F}}(R,Q,\lambda) \qquad \text{or} \qquad \mathrm{Ca} \gtrless \mathrm{Ca}_E\,\widetilde{\mathscr{F}}(R,Q,\lambda), \tag{31}$$

respectively. When $\mathrm{Ca}_E = 0$, (31) simplifies to $\mathrm{Ca} = 0$ or $\mathrm{Ca} \gtrless 0$, respectively, and when $\mathrm{Ca} = 0$, it yields the Taylor condition [37]: the drop remains spherical when $\mathscr{F} = 0$ and becomes prolate/oblate when $\mathscr{F} \gtrless 0$.

4. Spheroidal drop. Suppose the drop has a spheroidal shape, is centered at the origin, and has the axis of revolution coinciding with the z-axis. In the prolate spheroidal coordinates (ξ,η) related to the cylindrical coordinates as

$$r = c\,\sinh\xi\sin\eta, \qquad z = c\,\cosh\xi\cos\eta, \qquad \xi\in[0,\infty), \quad \eta\in[0,\pi], \tag{32}$$

where c is a metric parameter, ℓ is determined by fixing the coordinate ξ, i.e., $\xi = t$. In this case, the derivatives $\partial/\partial s$ and $\partial/\partial n$ on ℓ are determined by

$$\frac{\partial}{\partial s} = -\frac{1}{c\sqrt{\cosh^2\xi - \cos^2\eta}}\,\frac{\partial}{\partial\eta}, \qquad \frac{\partial}{\partial n} = \frac{1}{c\sqrt{\cosh^2\xi - \cos^2\eta}}\,\frac{\partial}{\partial\xi}.$$

In fact, it will be shown that the approach works for both prolate and oblate spheroids.

In the prolate spheroidal coordinates (32), the stream function Ψ^∞ takes the form

$$\Psi^\infty = -G\,r\,z = \frac{G\,c^2}{9}\mathrm{P}_2^{(1)}(\cosh\xi)\,\mathrm{P}_2^{(1)}(\cos\eta),$$

which suggests that the particular solution that solves the boundary conditions (23) and (26) with zero right-hand sides can be sought in the form

$$\Psi_0^\pm = G\,(\lambda-1)\left(z\,\Phi_0^\pm + \Omega_0^\pm\right), \tag{33}$$

with

$$\Phi_0^\pm(\xi,\eta) = c\;A_0^\pm\,\Theta_1^\pm(\xi)\,\mathrm{P}_1^{(1)}(\cos\eta), \qquad \Omega_0^\pm(\xi,\eta) = c^2\,B_0^\pm\,\Theta_2^\pm(\xi)\,\mathrm{P}_2^{(1)}(\cos\eta), \tag{34}$$

where $A_0^\pm$ and $B_0^\pm$ are unknown real-valued coefficients and

$$\Xi_n^+(\xi) = \mathrm{P}_n(\cosh\xi), \qquad \Theta_n^+(\xi) = \mathrm{P}_n^{(1)}(\cosh\xi),$$
$$\Xi_n^-(\xi) = \mathrm{Q}_n(\cosh\xi), \qquad \Theta_n^-(\xi) = \mathrm{Q}_n^{(1)}(\cosh\xi),$$

with $\mathrm{P}_n^{(k)}(\cosh\xi)$ and $\mathrm{Q}_n^{(k)}(\cosh\xi)$ being the associated Legendre functions of the first and second kinds, respectively (for $k=0$, the superscript is omitted). For brevity, let

$$a=\sinh t,\qquad b=\cosh t,\qquad d=\coth t.$$

It follows from (23) and (26) that

(35)
$$A_0^+=\frac{8}{\lambda W}\left(3(a^2+b^2)-1-6a^2b\ln\left[d+\frac{1}{a}\right]\right),\quad A_0^-=-\frac{48\,a^2b}{W},\quad B_0^-=\frac{16\,a^2b^3}{W},$$
$$B_0^+=\frac{8}{9\lambda W}\left(1-3(a^2+b^2)-18\lambda a^2b^2+3a^2b(2+\lambda+3\lambda(a^2+b^2))\ln\left[d+\frac{1}{a}\right]\right),$$
$$W=3(\lambda-1)\left(6\cosh[4t]+(2b+\cosh[3t]-3\cosh[5t])\ln\left[d+\frac{1}{a}\right]\right)-2(7+9\lambda).$$

Consequently,

$$\Psi^\pm=\Psi_0^\pm+\widehat{\Psi}^\pm, \tag{36}$$

where $\widehat{\Psi}^\pm$ satisfies (23) and (26) in place of $\Psi^\pm$ without Ψ^∞. Let $\widehat{\Psi}^\pm$ be represented by (25) in place of $\Psi^\pm$, and let the functions $\Phi^\pm$ and $\Omega^\pm$ in (25) be expanded into series of spheroidal harmonics (Legendre series):

$$\Phi^\pm(\xi,\eta)=\sum_{n=1}^{\infty}A_n^\pm\,\Theta_n^\pm(\xi)\,\mathrm{P}_n^{(1)}(\cos\eta),\quad \Omega^\pm(\xi,\eta)=c\sum_{n=1}^{\infty}B_n^\pm\,\Theta_n^\pm(\xi)\,\mathrm{P}_n^{(1)}(\cos\eta). \tag{37}$$

Let also

$$F_1=\sum_{n=1}^{\infty}g_n\,\mathrm{P}_n^{(1)}(\cos\eta),\qquad F_2=\sum_{n=1}^{\infty}h_n\,\mathrm{P}_n(\cos\eta). \tag{38}$$

With the relationship $x\,\mathrm{P}_n^{(1)}(x)=\frac{n}{2n+1}\,\mathrm{P}_{n+1}^{(1)}(x)+\frac{n+1}{2n+1}\,\mathrm{P}_{n-1}^{(1)}(x)$, $x\in[-1,1]$, the velocity boundary conditions (23) with $C_\psi=0$ yield

(39)
$$\left[b\left(\frac{n-1}{2n-1}\,\Theta_{n-1}^*(t)A_{n-1}^*+\frac{n+2}{2n+3}\,\Theta_{n+1}^*(t)A_{n+1}^*\right)+\Theta_n^*(t)B_n^*\right]\Big|_-^+=0,$$
$$\left[\frac{n-1}{2n-1}\left(b\,\Theta_{n-1}^*(t)\right)_t'\,A_{n-1}^*+\frac{n+2}{2n+3}\left(b\,\Theta_{n+1}^*(t)\right)_t'\,A_{n+1}^*+(\Theta_n^*(t))_t'\,B_n^*\right]\Big|_-^+=0,$$

where both equations hold for $n\geqslant 1$ and where $(\cdot)_t'$ denotes the derivative with respect to t. Then with

$$\widetilde{\Phi}^\pm(t,\eta)=-\int\frac{\partial\Phi^\pm(t,\eta)}{\partial t}\,d\eta=-\sum_{n=1}^{\infty}A_n^\pm\,\left(\Theta_n^\pm(t)\right)_t'\,\mathrm{P}_n(\cos\eta)+C,$$

where the constant of integration C is put to zero, and with the relationships $x\,\mathrm{P}_n(x)=\frac{n+1}{2n+1}\mathrm{P}_{n+1}(x)+\frac{n}{2n+1}\mathrm{P}_{n-1}(x)$ and $\sqrt{1-x^2}\,\mathrm{P}_n(x)=\frac{1}{2n+1}\left[\mathrm{P}_{n-1}^{(1)}(x)-\mathrm{P}_{n+1}^{(1)}(x)\right]$, $x\in[-1,1]$, the stress boundary conditions (26) yield

$$[\mu^*\,K_1^*\,A_1^*]|_-^+=-2b\,g_1-a\,h_1, \tag{40}$$

$$\begin{aligned}\left[\mu^*\left(\frac{2}{5}K_2^*A_2^*+2\,\Theta_1^*(t)B_1^*\right)\right]\Big|_-^+ &= -\frac{6}{5}b\,g_2-\frac{2}{5}a\,h_2,\\ [\mu^*(M_1^*A_2^*+2\,\Xi_1^*(t)B_1^*)]|_-^+ &= \frac{3}{5}a\,g_2+\frac{1}{5}b\,h_2,\end{aligned}\tag{41}$$

$$\begin{aligned}&\left[\mu^*\left(\frac{n}{2n-1}K_{n-1}^*A_{n-1}^*+\frac{n+1}{2n+3}K_{n+1}^*A_{n+1}^*+n(n+1)\,\Theta_n^*(t)B_n^*\right)\right]\Big|_-^+\\ &=b\left(\frac{n(n-1)}{2n-1}g_{n-1}-\frac{(n+1)(n+2)}{2n+3}g_{n+1}\right)-a\left(\frac{n\,h_{n-1}}{2n-1}+\frac{(n+1)\,h_{n+1}}{2n+3}\right),\\ &\qquad\qquad n\geqslant 2,\end{aligned}\tag{42}$$

$$\begin{aligned}&\left[\mu^*\left(L_n^*A_{n-1}^*+M_n^*A_{n+1}^*+n(n+1)\,\Xi_n^*(t)B_n^*\right)\right]\Big|_-^+\\ &\quad=a\left(\frac{n-1}{2n-1}g_{n-1}+\frac{n+2}{2n+3}g_{n+1}\right)-b\left(\frac{h_{n-1}}{2n-1}-\frac{h_{n+1}}{2n+3}\right),\quad n\geqslant 2,\end{aligned}\tag{43}$$

in which

$$\begin{aligned}K_n^{\pm}&=\left(n^2-1\right)b\,\Theta_n^{\pm}(t)+n\,\Theta_{n+1}^{\pm}(t),\\ L_n^{\pm}&=\frac{b}{2n-1}\left(n^2(n-1)\,\Xi_{n-1}^{\pm}(t)-d\,\Theta_{n-1}^{\pm}(t)\right),\\ M_n^{\pm}&=\frac{b}{2n+3}\left((n+1)^2(n+2)\,\Xi_{n+1}^{\pm}(t)+d\,\Theta_{n+1}^{\pm}(t)\right).\end{aligned}$$

With the relationship $\Theta_n^+(t)\,\Xi_n^-(t)-\Theta_n^-(t)\,\Xi_n^+(t)=1/a$, the system (39) yields

$$\begin{bmatrix}B_n^+\\ B_n^-\end{bmatrix}=\frac{a}{n(n+1)}\left(\left(\mathscr{K}_{n+1}-\mathscr{N}_{n+1}^+\right)\begin{bmatrix}\widetilde{A}_{n+1}^+\\ \widetilde{A}_{n+1}^-\end{bmatrix}-\left(\mathscr{K}_{n-1}+\mathscr{N}_{n-1}^-\right)\begin{bmatrix}\widetilde{A}_{n-1}^+\\ \widetilde{A}_{n-1}^-\end{bmatrix}\right),\quad n\geqslant 1,\tag{44}$$

and (42) and (43) can also be solved for B_n^+ and B_n^-:

$$\begin{aligned}\begin{bmatrix}B_n^+\\ B_n^-\end{bmatrix}&=\frac{a}{n(n+1)}\left(\left(\mathscr{L}_{n+1}-\mathscr{N}_{n+1}^+\right)\begin{bmatrix}\widetilde{A}_{n+1}^+\\ \widetilde{A}_{n+1}^-\end{bmatrix}-\left(\mathscr{L}_{n-1}+\mathscr{N}_{n-1}^-\right)\begin{bmatrix}\widetilde{A}_{n-1}^+\\ \widetilde{A}_{n-1}^-\end{bmatrix}\right)\\ &\quad+\frac{a}{n(n+1)\mu^+}\left(\mathscr{R}_{n-1}\begin{bmatrix}g_{n-1}\\ h_{n-1}\end{bmatrix}-\mathscr{R}_{n+1}\begin{bmatrix}g_{n+1}\\ h_{n+1}\end{bmatrix}\right),\quad n\geqslant 2,\end{aligned}\tag{45}$$

where

$$\widetilde{A}_n^{\pm}=\frac{n(n+1)}{2n+1}A_n^{\pm},\qquad \mathscr{K}_n=\begin{bmatrix}\frac{1}{a}+\alpha_n & -\delta_n^-\\ \delta_n^+ & -\alpha_n\end{bmatrix},\qquad \mathscr{L}_n=\begin{bmatrix}\beta_n & -\frac{\widetilde{\delta}_n^-}{\lambda}\\ \lambda\,\widetilde{\delta}_n^+ & \frac{1}{a}-\beta_n\end{bmatrix},$$

$$\mathscr{N}_n^+=\frac{b^2}{a}\begin{bmatrix}n & 0\\ 0 & n+1\end{bmatrix},\quad \mathscr{N}_n^-=\frac{b^2}{a}\begin{bmatrix}n+1 & 0\\ 0 & n\end{bmatrix},$$

$$\mathscr{R}_n=\frac{1}{2n+1}\begin{bmatrix}n(n+1)\Xi_n^-(t) & \Theta_n^-(t)\\ \lambda\,n(n+1)\Xi_n^+(t) & \lambda\,\Theta_n^+(t)\end{bmatrix},$$

$$\alpha_n = \left(1+b^2\right)\Xi_n^+(t)\,\Theta_n^-(t) + a\,b\left(\Theta_n^+(t)\,\Theta_n^-(t) - n(n+1)\,\Xi_n^+(t)\Xi_n^-(t)\right),$$
$$\delta_n^\pm = \left(1+b^2\right)\Xi_n^\pm(t)\,\Theta_n^\pm(t) + a\,b\left(\left(\Theta_n^\pm(t)\right)^2 - n(n+1)\left(\Xi_n^\pm(t)\right)^2\right),$$

$$\beta_n = \alpha_n + \left(\frac{d}{n(n+1)}\Theta_n^+(t) - 2\,\Xi_n^+(t)\right)\Theta_n^-(t),$$
$$\widetilde{\delta}_n^\pm = \delta_n^\pm + \left(\frac{d}{n(n+1)}\Theta_n^\pm(t) - 2\,\Xi_n^\pm(t)\right)\Theta_n^\pm(t).$$

Equating (44) and (45), we obtain

$$\begin{bmatrix}\widehat{A}_{n+1}^+ - \widehat{A}_{n-1}^+\\ \widehat{A}_{n+1}^- - \widehat{A}_{n-1}^-\end{bmatrix} = \frac{1}{\mu^+}\left(\mathscr{R}_{n-1}\begin{bmatrix}g_{n-1}\\ h_{n-1}\end{bmatrix} - \mathscr{R}_{n+1}\begin{bmatrix}g_{n+1}\\ h_{n+1}\end{bmatrix}\right), \quad n = 2,4,6,\ldots, \tag{46}$$

where

$$\begin{bmatrix}\widehat{A}_n^+\\ \widehat{A}_n^-\end{bmatrix} = \mathscr{M}_n\begin{bmatrix}\widetilde{A}_n^+\\ \widetilde{A}_n^-\end{bmatrix}, \qquad \mathscr{M}_n = \begin{bmatrix}\alpha_n - \beta_n + \dfrac{1}{a} & \dfrac{\widetilde{\delta}_n^-}{\lambda} - \delta_n^-\\ \delta_n^+ - \lambda\,\widetilde{\delta}_n^+ & \beta_n - \alpha_n - \dfrac{1}{a}\end{bmatrix}.$$

First-order difference equation (46) implies that $\widehat{A}_1^\pm, \widehat{A}_3^\pm, \widehat{A}_5^\pm, \ldots$ are determined by

$$\begin{bmatrix}\widehat{A}_n^+\\ \widehat{A}_n^-\end{bmatrix} = -\frac{1}{\mu^+}\mathscr{R}_n\begin{bmatrix}g_n\\ h_n\end{bmatrix} + \begin{bmatrix}q^+\\ q^-\end{bmatrix}, \quad n = 1,3,5\ldots, \tag{47}$$

where $q^\pm$ are unknown constants related through (40). A solution for $\widehat{A}_2^\pm, \widehat{A}_4^\pm, \widehat{A}_6^\pm, \ldots$ has a similar form, where this time $q^\pm$ are determined from (41). With (47), the left-hand side of (40) can be written as

$$[\mu^*\,K_1^*\,A_1^*]|_-^+ = \mu^-\left(\lambda\,K_1^+, -K_1^-\right)\begin{bmatrix}A_1^+\\ A_1^-\end{bmatrix} = \frac{3}{2}\mu^-\underbrace{\left(\lambda\,K_1^+, -K_1^-\right)\mathscr{M}_1^{-1}}_{=(0,2)}\begin{bmatrix}\widehat{A}_1^+\\ \widehat{A}_1^-\end{bmatrix} = 3\mu^-\widehat{A}_1^-$$
$$= -(2b\,g_1 + a\,h_1) + 3\mu^- q^-,$$

which, being compared to the right-hand side of (40), implies that $q^- = 0$, whereas q^+ can be arbitrary. Let $q^+ = 0$; then the coefficients $A_1^\pm, A_3^\pm, A_5^\pm, \ldots$ are given by

$$\begin{bmatrix}A_n^+\\ A_n^-\end{bmatrix} = -\frac{2n+1}{n(n+1)\mu^+}\mathscr{M}_n^{-1}\mathscr{R}_n\begin{bmatrix}g_n\\ h_n\end{bmatrix}, \quad n = 1,3,5\ldots, \tag{48}$$

with

$$\mathscr{M}_n^{-1} = -\frac{\mathscr{M}_n}{\det\mathscr{M}_n}, \qquad \det\mathscr{M}_n = (\lambda-1)\left(\lambda^{-1}\delta_n^+\,\widetilde{\delta}_n^- - \delta_n^-\,\widetilde{\delta}_n^+\right) - \frac{1}{a^2},$$

and the coefficients $B_2^\pm, B_4^\pm, B_6^\pm, \ldots$ are determined by (44). Observe that the solution (48) is nonrecursive and holds for an arbitrary axisymmetric vector $\mathbf{F}$ in (5). The coefficients $A_2^\pm, A_4^\pm, A_6^\pm, \ldots$ are determined similarly.

In the case of $\lambda = 1$, the solution (48) simplifies to

$$\begin{bmatrix}A_n^+\\ A_n^-\end{bmatrix} = \frac{a}{n(n+1)\mu^+}\begin{bmatrix}d\,\Theta_n^-(t) - n(n+1)\Xi_n^-(t) & \Theta_n^-(t)\\ d\,\Theta_n^+(t) - n(n+1)\Xi_n^+(t) & \Theta_n^+(t)\end{bmatrix}\begin{bmatrix}g_n\\ h_n\end{bmatrix}, \quad n = 1,3,5\ldots.$$

4.1. Oblate spheroidal drop. The obtained solution holds for oblate spheroids as well. Since the spheroidal drop is assumed to have fixed volume of $4\pi l^3/3$, it has a single free parameter, which we choose to be the axes ratio $d = \coth t$, where $d > 1$ and $d < 1$ correspond to prolate and oblate spheroids, respectively. In both cases $d > 1$ and $d < 1$, the metric parameter c in (32) and the value t that determines the spheroid's surface can be defined by $c = l\, d^{-1/3}\sqrt{d^2-1}$ and $t = \operatorname{arccoth} d$, respectively. For $d < 1$, c is imaginary and t has the complex part of $-\pi/2$, but $r = c \sinh t \sin\eta$ and $z = c \cosh t \cos\eta$ remain real, and $(\xi - \mathrm{i}\pi/2, \eta)$ with imaginary c correspond to oblate spheroidal coordinates.

4.2. Particular solution corresponding to $\mathbf{F}_\gamma \equiv -\gamma\, \mathfrak{n} \operatorname{div} \mathfrak{n}$. For $\mathbf{F} = \mathbf{F}_\gamma \equiv -\gamma\, \mathfrak{n} \operatorname{div} \mathfrak{n}$, the functions F_1 and F_2 are defined by (20) with $\widetilde{C}_1 = 0$ and $\widetilde{C}_2 = 0$, respectively, and the coefficients in their Legendre series (38) are determined by

$$g_n = \gamma\, \frac{2n+1}{4n(n+1)}\, b\, J_n^{(1)}, \qquad h_n = -\gamma\, \frac{2n+1}{4}\, a\, J_n^{(0)},$$

with

$$J_n^{(0)} = \int_{-1}^{1} \frac{x\, \mathrm{P}_n(x)}{\sqrt{b^2 - x^2}}\, dx, \qquad J_n^{(1)} = \int_{-1}^{1} \frac{\sqrt{1-x^2}\, \mathrm{P}_n^{(1)}(x)}{\sqrt{b^2 - x^2}}\, dx \tag{49}$$

being evaluated recursively by

$$\begin{aligned} J_{2k+1}^{(0)} &= \frac{(4k+1)b^2 - 2k + 1}{2(k+1)}\, J_{2k-1}^{(0)} + \frac{(4k+1)b^2}{4k(k+1)}\, J_{2k-1}^{(1)}, \\ J_{2k+1}^{(1)} &= \frac{2k+1}{2(k+1)} \left((4k+1)\, a^2 J_{2k-1}^{(0)} + \frac{(4k+1)b^2 - 2k - 2}{2k}\, J_{2k-1}^{(1)} \right), \end{aligned} \tag{50}$$

where $J_1^{(0)} = b^2 \arcsin(1/b) - a$ and $J_1^{(1)} = \left(b^2 - 2\right) \arcsin(1/b) - a$; see *section* S2 *in the supplementary materials* for the derivation of (50). The particular solution (48) that corresponds to $\mathbf{F} = \mathbf{F}_\gamma \equiv -\gamma\, \mathfrak{n} \operatorname{div} \mathfrak{n}$ is given by $A_n^{\pm} = (\gamma/\mu^-)\, A_n^{\gamma,\pm}$, $n = 1, 3, 5 \ldots$, where

$$\begin{bmatrix} A_n^{\gamma,+} \\ A_n^{\gamma,-} \end{bmatrix} = \frac{2n+1}{4n(n+1)\lambda} \mathscr{M}_n^{-1} \begin{bmatrix} a\, \Theta_n^-(t) & -b\, \Xi_n^-(t) \\ \lambda\, a\, \Theta_n^+(t) & -\lambda\, b\, \Xi_n^+(t) \end{bmatrix} \begin{bmatrix} J_n^{(0)} \\ J_n^{(1)} \end{bmatrix}, \quad n = 1, 3, 5 \ldots. \tag{51}$$

4.3. Particular solution corresponding to $\mathbf{F}_E$. On the surface of a spheroidal drop with axes ratio d, the normal and tangential components of the electric field E_n^- and E_t^- are determined in the prolate spheroidal coordinates (32) by

$$E_n^-\big|_{\xi=t} = \frac{E_\infty \cos\eta}{\mathcal{D}\sqrt{b^2 - \cos^2\eta}}, \qquad E_t^-\big|_{\xi=t} = \frac{E_\infty R\, d\, \sin\eta}{\mathcal{D}\sqrt{b^2 - \cos^2\eta}}, \tag{52}$$

with $t = \operatorname{arccoth} d$ and $\mathcal{D} = a\, \Xi_1^-(t) - R\, b\, \Theta_1^-(t)$ (see, e.g., [48]), and $\mathbf{F}_E$ in (7) takes the form

$$\mathbf{F}_E = \frac{\varkappa}{2\mathcal{D}^2} \left[\frac{R(1-QR)d \sin 2\eta}{b^2 - \cos^2\eta}\, \mathfrak{s} + \left[QR^2 - 1 + (Q-1)R^2 d^2 - b^2 \frac{(2Q-1)R^2 - 1}{b^2 - \cos^2\eta} \right] \mathfrak{n} \right], \tag{53}$$

where $\varkappa = \varepsilon_0\, \varepsilon^-\, E_\infty^2$. The representations (52) and (53) hold for both prolate ($d > 1$) and oblate ($d < 1$) spheroids.

The coefficients g_n and h_n in (48) that correspond to $\mathbf{F}_E$ are given by

$$
\begin{aligned}
&g_1 = \varkappa\left(\widetilde{g} + (R-1)^2\,\widehat{g}_1\right), \qquad \widetilde{g} = -\frac{c}{8\mathcal{D}^2 a}\left(QR^2 - 1 + (R-1)^2\,b^2\right),\\
&g_n = \varkappa\,(R-1)^2\,\widehat{g}_n, \qquad \widehat{g}_n = -\frac{a\,b^2 c}{8\mathcal{D}^2}\,I_n\,\Xi_n^-(t), \quad n \geqslant 1,
\end{aligned}
\tag{54}
$$

$$
\begin{aligned}
&h_1 = \varkappa\left(\widetilde{h} + (R-1)^2\,\widehat{h}_1\right), \qquad \widetilde{h} = -\frac{b\,c}{8\mathcal{D}^2}\left(\frac{R(R-3QR+2)}{a^2} + (R-1)^2\right),\\
&h_n = \varkappa\,(R-1)^2\,\widehat{h}_n, \qquad \widehat{h}_n = \frac{b^2 c}{8\mathcal{D}^2}\,I_n\left(a\,\Theta_n^-(t) + b\,\Xi_n^-(t)\right), \quad n \geqslant 1.
\end{aligned}
\tag{55}
$$

For the derivation of g_n and h_n, see *section* S3 *in the supplementary materials.*

Thus, the particular solution (48) that corresponds to $\mathbf{F}_E$ is given by $A_n^{\pm} = (\varkappa/\mu^-)\,A_n^{E,\pm}$, $n = 1, 3, 5\ldots$, where

$$
\begin{bmatrix} A_n^{E,+} \\ A_n^{E,-} \end{bmatrix} = -\frac{2n+1}{n(n+1)\,\lambda\,\varkappa}\mathscr{M}_n^{-1}\mathscr{R}_n\begin{bmatrix} g_n \\ h_n \end{bmatrix}, \quad n = 1, 3, 5\ldots,
\tag{56}
$$

with g_n and h_n determined by (54) and (55), respectively.

4.4. Spheroidal drop under presence of aligned linear flow and uniform electric field. Under the presence of the aligned linear flow $\mathbf{u}^\infty$ and uniform electric field $\mathbf{E}^\infty$, the stream functions $\Psi^\pm$ are determined by (36), where $\Psi_0^\pm$ are given by (33) and $\widehat{\Psi}^\pm$ are represented by (25) in place of $\Psi^\pm$ with the functions $\Phi^\pm$ and $\Omega^\pm$ in the series form (37), in which $A_n^\pm$ are determined by

$$
A_n^{\pm} = \frac{\gamma}{\mu^-}A_n^{\gamma,\pm} + \frac{\varkappa}{\mu^-}A_n^{E,\pm}, \qquad n = 1, 3, 5\ldots,
\tag{57}
$$

with $A_n^{\gamma,\pm}$ and $A_n^{E,\pm}$ given by (51) and (56), respectively, and $B_n^\pm$ follow from (44).

The dimensions (r and z), $\mathbf{E}^\pm$, $\mathbf{u}^\infty + \mathbf{u}^\pm$, and $p^\pm$ are now rescaled by l, E_∞, U, and $\varkappa$, respectively, where $U = \varkappa l/\mu^-$ is a characteristic velocity. With the electric capillary number $\mathrm{Ca}_E = \varkappa l/\gamma$ and the capillary number $\mathrm{Ca} = \mu^- G l/\gamma$, the total stream function $\Psi^\infty + \Psi^+$ on ℓ can be represented in dimensionless form by

$$
\begin{aligned}
\left(\Psi^\infty + \Psi^+\right)\big|_{\xi=t} &= \left(\Psi^\infty + \Psi_0^+ + \widehat{\Psi}^+\right)\Big|_{\xi=t}\\
&= \frac{\mathrm{Ca}}{\mathrm{Ca}_E}\,f^G\,\mathrm{P}_2^{(1)}(\cos\eta) + \sum_{k=1}^{\infty}\left(\frac{f_k^\gamma}{\mathrm{Ca}_E} + f_k^E\right)\mathrm{P}_{2k}^{(1)}(\cos\eta),
\end{aligned}
\tag{58}
$$

where $f^G = -32abc^2/(3W)$ with W defined in (35) and

$$
f_k^j = b\,c\left(\frac{2k-1}{4k-1}\,\Theta_{2k-1}^+(t)A_{2k-1}^{j,+} + \frac{2k+2}{4k+3}\,\Theta_{2k+1}^+(t)A_{2k+1}^{j,+}\right) + c\,\Theta_{2k}^+(t)B_{2k}^{j,+}, \quad k \geqslant 1,
\tag{59}
$$

in which j stands for "γ" and "E," and $B_n^{j,+}$ are determined by (44) with $A_n^\pm$ replaced by $A_n^{j,\pm}$ for $j =$"γ" and "E."

The spheroidal drop of fixed volume has the single free parameter d (axes ratio), and consequently it may not satisfy the kinematic condition (24) exactly; i.e., (58)

may not vanish for all $\eta \in [0,\pi]$. For each $\mathrm{Ca} \in \mathbb{R}$ and $\mathrm{Ca}_E \geqslant 0$, the "steady" spheroid can be defined as the one that minimizes the square error

$$\begin{aligned}\mathcal{E}(d) &= \|\Psi^+ + \Psi^\infty\|^2 = \mathrm{Ca}_E^2 \int_0^\pi (\Psi^+ + \Psi^\infty)^2 \sin\eta \, d\eta \\ &= \left(\mathrm{Ca}\, f^G + \mathrm{Ca}_E\, f_1^E + f_1^\gamma\right)^2 w_1 + \sum_{k=2}^{\infty} \left(f_k^\gamma + \mathrm{Ca}_E\, f_k^E\right)^2 w_k,\end{aligned} \tag{60}$$

with respect to d, where $w_k = 4k(2k+1)/(4k+1)$ and the multiplier Ca_E^2 is introduced to make the error finite for $\mathrm{Ca}_E = 0$. However, a numerically found minimizer of $\mathcal{E}(d)$ would not provide an analytical insight into the interplay of Ca, Ca_E, R, Q, and λ for "steady" spheroids. So, the analysis can be simplified as follows.

Observe that through (59) and (56), the coefficients f_k^E are determined by $g_n/\varkappa$ and $h_n/\varkappa$ in (54) and (55). They can be represented as

$$f_1^E = \widetilde{f} + (R-1)^2 \widehat{f}_1, \qquad f_k^E = (R-1)^2 \widehat{f}_k, \quad k \geqslant 2,$$

where $\widetilde{f}$ and $\widehat{f}_k$ correspond to $\widetilde{g}$ and $\widetilde{h}$ and to $\widehat{g}_n$ and $\widehat{h}_n$, respectively, in (54) and (55). The significance of f_k^γ and $\widehat{f}_k$, $k \geqslant 2$, with respect to f_1^γ and $\widehat{f}_1$, respectively, can be measured by the ratios

$$\epsilon_\gamma = \frac{\sum_{k=2}^{\infty} \left(f_k^\gamma\right)^2 w_k}{\left(f_1^\gamma\right)^2 w_1}, \qquad \epsilon_E = \frac{\sum_{k=2}^{\infty} \left(\widehat{f}_k\right)^2 w_k}{\left(\widehat{f}_1\right)^2 w_1}, \tag{61}$$

which are both independent of R and Q.[5] Figure 1 shows ϵ_γ and ϵ_E versus the Taylor deformation parameter $D = (d-1)/(d+1)$ for $\lambda = 0.01$, 0.1, 1, and 100.

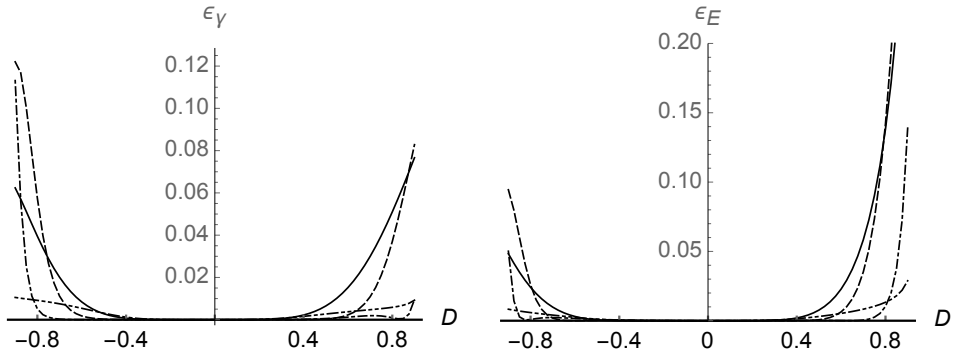

FIG. 1. *Ratios ϵ_γ and ϵ_E, defined by* (61) *and measuring the significance of f_k^γ and $\widehat{f}_k$, $k \geqslant 2$, with respect to f_1^γ and $\widehat{f}_1$, respectively, versus the Taylor deformation parameter D for $\lambda = 0.01$ (dot-dashed curves),* 0.1 *(dashed curves),* 1 *(solid curves), and* 100 *(double-dot-dashed curves).*

Let $\bar{\epsilon}_\gamma$ and $\bar{\epsilon}_E$ be upper bounds on ϵ_γ and ϵ_E, respectively, for a certain range of d (or D) and for all λ of interest. For example, $\bar{\epsilon}_\gamma = 0.003$ and $\bar{\epsilon}_E = 0.002$ for $D \in [-0.5, 0.4]$, and $\bar{\epsilon}_\gamma = 0.009$ and $\bar{\epsilon}_E = 0.008$ for $D \in [-0.6, 0.5]$ for all $\lambda = 0.01$, 0.1, 1, and 100. Then (60) is bounded from above by

$$\left(\mathrm{Ca}\, f^G + \mathrm{Ca}_E \left(\widetilde{f} + (R-1)^2 \widehat{f}_1\right) + f_1^\gamma\right)^2 w_1 + 2\left(\left(f_1^\gamma\right)^2 \bar{\epsilon}_\gamma + \mathrm{Ca}_E^2 (R-1)^4 \left(\widehat{f}_1\right)^2 \bar{\epsilon}_E\right) w_1. \tag{62}$$

[5] Observe that $\widehat{f}_k$ depends on R through $\mathcal{D}$ in $\widehat{g}_k$ and $\widehat{h}_k$, but $\mathcal{D}$ is canceled out in the ratio ϵ_E.

When $\bar{\epsilon}_\gamma \ll 1$ and $\bar{\epsilon}_E \ll 1$, which is the case at least for $D \in [-0.5, 0.4]$ and $\lambda = 0.01$, 0.1, 1, and 100, the second term in (62) can be omitted,[6] and minimization of the first one with respect to d yields

$$\mathrm{Ca} = -\left(\mathrm{Ca}_E f_1^E + f_1^\gamma\right)/ f^G. \tag{63}$$

However, not all d, Ca, and Ca_E related by (63) may be feasible since a spherical drop becomes prolate/oblate if $\mathrm{Ca} \gtrless \mathrm{Ca}_E \widetilde{\mathscr{F}}(R, Q, \lambda)$, where $\widetilde{\mathscr{F}}(R, Q, \lambda)$ is defined by (29). This condition can be written as $(d-1)(\mathrm{Ca} - \mathrm{Ca}_E \widetilde{\mathscr{F}}(R, Q, \lambda)) > 0$, and with (63) and the fact that $f^G \gtrless 0$ if $d \gtrless 1$, it yields a condition for feasible $\mathrm{Ca}_E \geqslant 0$ and d:

$$\left(f^G \widetilde{\mathscr{F}}(R, Q, \lambda) + f_1^E\right) \mathrm{Ca}_E + f_1^\gamma < 0. \tag{64}$$

In this case, the Taylor deformation parameter D for "steady" spheroids as a function of Ca and Ca_E, to be referred to as deformation surface, is determined parametrically by

$$\left(-\frac{\mathrm{Ca}_E f_1^E + f_1^\gamma}{f^G}, \mathrm{Ca}_E, \frac{d-1}{d+1}\right), \tag{65}$$

where $d > 0$ and $\mathrm{Ca}_E \geqslant 0$ are parameters and are feasible if they satisfy (64). For (65), the error $\mathcal{E}$ is bounded from above by the second term in (62).

The relationship (63) "generalizes" the first condition in (31) for spheroidal drops and has the following interpretation. Let $\mathrm{Ca}^*(d)$ and $\mathrm{Ca}_E^*(d)$ be the values of Ca and Ca_E for which a spheroid with axes ratio d is "steady" when the linear flow and electric field are applied separately, respectively; i.e., in the cases of $\mathrm{Ca}_E = 0$ and of $\mathrm{Ca} = 0$, (63) implies that

$$\mathrm{Ca}^*(d) = -f_1^\gamma / f^G, \qquad \mathrm{Ca}_E^*(d) = -f_1^\gamma / f_1^E. \tag{66}$$

Then (63) can be recast in the form

$$\frac{\mathrm{Ca}}{\mathrm{Ca}^*(d)} + \frac{\mathrm{Ca}_E}{\mathrm{Ca}_E^*(d)} = 1, \tag{67}$$

which unifies the cases of separately applied linear flow and uniform electric field: $\mathrm{Ca} = \mathrm{Ca}^*(d) \Longleftrightarrow \mathrm{Ca}_E = 0$ and $\mathrm{Ca}_E = \mathrm{Ca}_E^*(d) \Longleftrightarrow \mathrm{Ca} = 0$. In (67), $\mathrm{Ca}/\mathrm{Ca}^*(d)$ and $\mathrm{Ca}_E/\mathrm{Ca}_E^*(d)$ can be viewed as "percentages" that the linear flow and electric field contribute to the stability of a spheroid with axes ratio d; i.e., Ca and Ca_E need to be measured in "units" of $\mathrm{Ca}^*(d)$ and $\mathrm{Ca}_E^*(d)$ to be treated on the "same scale." When $d \to 1$, $\mathrm{Ca}^*(d) \to 0$ and $\mathrm{Ca}_E^*(d) \to 0$, and (67) with the first condition in (31) yields

$$-\lim_{d\to 1} \frac{\mathrm{Ca}^*(d)}{\mathrm{Ca}_E^*(d)} = \frac{\mathrm{Ca}}{\mathrm{Ca}_E} = \widetilde{\mathscr{F}}(R, Q, \lambda). \tag{68}$$

Strictly speaking, $\mathrm{Ca}_E^*(d)$ in (66) corresponds to a "steady" spheroid under the presence of only the electric field only when it is positive, i.e., when $\mathscr{F}(R, Q, \lambda) \gtrless 0$ for

[6] The expression (62) can be written as $\left(\mathrm{Ca}^2 \left(f^G\right)^2 + \mathrm{Ca}_E^2 \left(\widetilde{f}\right)^2 + \mathrm{Ca}_E^2 (R-1)^4 \left(\widehat{f}_1\right)^2 (1 + 2\bar{\epsilon}_E) + \left(f_1^\gamma\right)^2 (1 + 2\bar{\epsilon}_\gamma) + \cdots\right) w_1$, where $\bar{\epsilon}_\gamma$ and $\bar{\epsilon}_E$ appear only in the multipliers $1 + 2\bar{\epsilon}_\gamma$ and $1 + 2\bar{\epsilon}_E$. Also, it may seem that for $R \gg 1$ the error is proportional to $(R-1)^4$; however, this is not the case since the denominator of $\widehat{f}_1$ contains $\mathcal{D}^2$, and $\mathcal{D}$ depends on R linearly, so the error is $O(1)$ as $R \to \infty$.

$d \gtrless 1$, where $\mathscr{F}$ is the Taylor discriminating function (30). Nevertheless, (67) holds regardless of this interpretation.

Yet another insight into (63) can be gained through the inverse problem that finds parameters of imposed (flow/electric) fields to make a drop with a given shape steady (if possible). Suppose that Ca_E is given; then Ca, for which a spheroidal drop with axes ratio d is "steady," minimizes the error (60) and is given by (63). Thus, (63) solves direct error minimization (direct problem) approximately, whereas it solves the inverse problem with respect to Ca exactly, and the residual error in both cases is the same. In general, deformation curves obtained from the direct and inverse problems with the same error do not coincide. However, the smaller the corresponding optimal values of the error are, the closer the curves are expected to be and coincide when the optimal values vanish provided that the curves are one-to-one correspondences. Similarly, when Ca is given, the inverse problem minimizes $\mathcal{E}$ with respect to $\mathrm{Ca}_E \geqslant 0$ and implies that (63) holds approximately. Thus, under the assumption of $\epsilon_\gamma \ll 1$ and $\epsilon_E \ll 1$, the relationship (63) can be used for finding any of the three Ca, Ca_E, and D when the other two are given, and the residual error is bounded above by the second term in (62). If the question is posed to find both Ca and Ca_E that make a spheroid with given axes ratio "steady," then for $R \neq 1$, minimization of the error (60) with respect to both Ca and Ca_E would yield $\mathrm{Ca}_E = -\sum_{k=2}^{\infty} f_k^\gamma f_k^E w_k / \sum_{k=2}^{\infty} \left(f_k^E\right)^2 w_k$ and Ca would still be determined by (63).

In fact, $\mathrm{Ca}^*(d)$ and $\mathrm{Ca}_E^*(d)$ can be expressed in elementary functions; however, the corresponding expressions are rather lengthy. For $\lambda = 1$, they are given by

$$
\begin{aligned}
\mathrm{Ca}^*(d) = \frac{15\, d^{1/3}}{2^9 \left(d^2-1\right)^{11/2}} \Bigg(& d\sqrt{d^2-1}\left(8 + 878\, d^2 + 695\, d^4 - 6\, d^6\right) \\
& + \left(8 - 194\, d^2 - 1053\, d^4 - 344\, d^6 + 8\, d^8\right) \ln\left[d + \sqrt{d^2-1}\right] \\
& + d^2 \arcsin\left[\sqrt{1-d^{-2}}\right] \Bigg(-3\, d\left(152 + 348\, d^2 + 23\, d^4 + 2\, d^6\right) \\
& + \frac{56 + 796\, d^2 + 723\, d^4 - 8\, d^6 + 8\, d^8}{\sqrt{d^2-1}} \ln\left[d + \sqrt{d^2-1}\right] \Bigg) \Bigg)
\end{aligned}
\tag{69}
$$

and

$$
\mathrm{Ca}_E^*(d) = \frac{384\left(d^2-1\right)^4 (p_0(d))^2\, \mathrm{Ca}^*(d)}{96\, R(QR-1)\, d(d^2-1)^{9/2} p_1(d) - 5(R-1)^2\, d^2 p_2(d)},
\tag{70}
$$

where

$$
\begin{aligned}
p_0(d) &= \left(R\, d^2 - 1\right)\sqrt{d^2-1} + (1-R)\, d \ln\left[d + \sqrt{d^2-1}\right], \\
p_1(d) &= 3d\sqrt{d^2-1} - \left(1 + 2d^2\right) \ln\left[d + \sqrt{d^2-1}\right], \\
p_2(d) &= d^2 q_0(d) - 6d\, q_1(d)\sqrt{d^2-1} \ln\left[d + \sqrt{d^2-1}\right] + 9 q_2(d) \left(\ln\left[d + \sqrt{d^2-1}\right]\right)^2,
\end{aligned}
$$

with $q_0(d) = 172\, d^6 + 984\, d^4 - 909\, d^2 - 247$, $q_1(d) = 16\, d^6 + 296\, d^4 + 210\, d^2 + 3$, and $q_2(d) = 64\, d^6 + 96\, d^4 + 16\, d^2 - 1$. Both (69) and (70) hold for $d > 1$ and for $d < 1$. For example, (69) has maximum and minimum values of 0.06 and -0.1916, which correspond to critical Ca in extensional and compressional flows, respectively (numerical results will be discussed in section 5).

For arbitrary λ, $\mathrm{Ca}^*(\cdot)$ and $\mathrm{Ca}^*_E(\cdot)$ can be readily expanded in terms of the Taylor deformation parameter D (higher-order terms are lengthy):

(71)
$$\mathrm{Ca}^*\left(\frac{1+D}{1-D}\right)=\frac{16(1+\lambda)}{3(16+19\,\lambda)}\,D-\frac{32\left(592+1961\,\lambda+1297\,\lambda^2\right)}{315(16+19\,\lambda)^2}\,D^2+O\big(D^3\big),$$
$$\mathrm{Ca}^*_E\left(\frac{1+D}{1-D}\right)=\frac{16}{9}\frac{(1+2R)^2}{\mathscr{F}(R,Q,\lambda)}\,D-\frac{32(1+2R)\sum_{k=0}^3\widehat{q}_k(\lambda)R^k}{4725(1+\lambda)^2\left(\mathscr{F}(R,Q,\lambda)\right)^2}\,D^2+O\big(D^3\big),$$

with $\widehat{q}_0(\lambda)=815(1+\lambda)^2$, $\widehat{q}_1(\lambda)=280+1751\,\lambda+1399\,\lambda^2$, $\widehat{q}_2(\lambda)=131+1132\,\lambda+857\,\lambda^2$ $-Q\left(2800+6791\,\lambda+3919\lambda^2\right)$, and $\widehat{q}_3(\lambda)=2Q\left(1232+2029\,\lambda+869\,\lambda^2\right)-890(1+\lambda)^2$. It follows from (71) that $\lim_{D\to0}\mathrm{Ca}^*/\mathrm{Ca}^*_E=-\widetilde{\mathscr{F}}(R,Q,\lambda)$, which proves (68).

The inverses of $\mathrm{Ca}^*(\cdot)$ and $\mathrm{Ca}^*_E(\cdot)$ in (71) imply that

(72)
$$D=\frac{3(16+19\,\lambda)}{16(1+\lambda)}\,\mathrm{Ca}\left(1+\frac{592+1961\,\lambda+1297\,\lambda^2}{280(1+\lambda)^2}\,\mathrm{Ca}\right)+O\big(\mathrm{Ca}^3\big),$$
$$D=\frac{9}{16}\frac{\mathscr{F}(R,Q,\lambda)}{(1+2R)^2}\,\mathrm{Ca}_E\left(1+\frac{3}{1400}\frac{\sum_{k=0}^3\widehat{q}_k(\lambda)R^k}{(1+2R)^3(1+\lambda)^2}\,\mathrm{Ca}_E\right)+O\big(\mathrm{Ca}_E^3\big)$$

for $|\mathrm{Ca}|\ll1$ and $\mathrm{Ca}_E\ll1$,[7] respectively. Both expressions in (72) agree with the linear theory [34, 37]. However, the first one differs from the $O(\mathrm{Ca}^2)$ theory [4] by[8]

(73)
$$-\frac{(16+19\,\lambda)(1392+16741\,\lambda+40923\,\lambda^2+15998\,\lambda^3)}{725760(1+\lambda)^3(3+2\,\lambda)}\,\mathrm{Ca}^2,$$

whereas the second one differs from the $O(\mathrm{Ca}_E^2)$ theory [2] by[9]

(74)
$$\frac{3}{8960}\frac{\mathscr{F}(R,Q,\lambda)}{(1+2R)^4}\left(15(R-1)^2+R(1-Q\,R)\frac{37\lambda-16}{\lambda+1}\right)\mathrm{Ca}_E^2.$$

The discrepancies (73) and (74) could be a result of replacing the error (60) by its upper bound (62) and may not be easy to detect numerically since the coefficient at Ca^2 in (73) is in the range $[-0.209,-0.01]$ and the one at Ca_E^2 in (74) is also small for moderate values of R, Q, and λ. Barthès-Biesel and Acrivos [4, p. 9] remarked that "the $O(\mathrm{Ca})$ results are slightly better than those of the $O(\mathrm{Ca}^2)$ theory for negative Ca. The difference, however, is not significant and may be due to the fact that ... the $O(\mathrm{Ca}^2)$ expression for the shape does not contain all the relevant terms." This could be yet another reason for the discrepancy with the $O(\mathrm{Ca}^2)$ theory.

With the slender-body analysis of drop deformation for $\lambda\to0$, Yariv and Rhodes [47, eq. (8.6)] obtained $\mathrm{Ca}_E\sim480^{1/3}R\big/\big((\pi^2(R+Q-6RQ+4)\big)\,d^{7/3}/\ln d$ as $d\to\infty$, whereas (66) for $\lambda\to0$ yields $\mathrm{Ca}_E\sim3\pi R\,/(64(1-RQ))\,d^{7/3}/\ln d$ as $d\to\infty$. Both results imply that $\mathrm{Ca}_E=\mathcal{O}\left(d^{7/3}/\ln d\right)$ as $d\to\infty$ and differ only in constants. When either $R=1$ or $Q=1$, the relative difference between the constants is 0.07742.

[7] The inverse of a series $a_1D+a_2D^2+O(D^3)$ as $D\to0$ is given by $a_1^{-1}\mathrm{Ca}-a_1^{-3}a_2\,\mathrm{Ca}^2+O(\mathrm{Ca}^3)$ as $\mathrm{Ca}\to0$. Substituting the latter into the former yields $\mathrm{Ca}+O(\mathrm{Ca}^3)$.

[8] In [4], F can be represented by $\sum_{k=0}^2 f_k\,\mathrm{Ca}^k+O(\mathrm{Ca}^2)$, with f_k found by satisfying (3.1) up to $O(\mathrm{Ca}^2)$. Exact roots of cubic equation (3.1) can be determined by the Cardano–Tartaglia formulas, and in the case of multiple real roots, the correct one is the closest to the asymptotic value $\sum_{k=0}^2 f_k\,\mathrm{Ca}^k$.

[9] The $O(\mathrm{Ca}_E^2)$ form of the Taylor deformation parameter D is given by equation (2.15) in [17].

5. Numerical results. The obtained solution for a spheroidal drop is first compared to the existing theoretical and experimental results in the cases of separately applied linear flow and uniform electric field and then is analyzed when the aligned linear flow and uniform electric field are applied in combination.

5.1. Spheroidal drop in extensional/compressional flow. In the presence of the linear flow only, $\mathrm{Ca}_E = 0$, and as a function of Ca, the Taylor deformation parameter D for "steady" spheroids (deformation curve) corresponds to the cross section of the deformation surface (65) at $\mathrm{Ca}_E = 0$. In the (Ca, D)-plane, it is plotted as $(\mathrm{Ca}^*((1+D)/(1-D)), D)$, where $\mathrm{Ca}^*(\cdot)$ is determined in (66). Figure 2 shows D versus Ca for "steady" spheroids and for boundary integral equation (BIE)-based steady shapes [25, 24, 51] for $\lambda = 0.01$, 0.1, 1, and 100. (In [24], Ca is defined as half of Ca here.) Figure 3 and Figure S2 *in the supplementary materials* compare "steady" spheroid deformation curves to those for BIE-based steady shapes [25, 24, 32, 51], to those predicted by the $O(\mathrm{Ca})$ and $O(\mathrm{Ca}^2)$ theories [34, 4], and to those for "steady" spheroids from [50, 51]. For $\lambda = 1$ and $\mathrm{Ca} \in [-0.5, 0.35]$, deformations of "steady" spheroids based on (69) are in remarkable agreement with those of BIE-based steady shapes [24, Duffy and Blundell],[10] [51]. Also, for $\lambda = 10, \infty$, and $\mathrm{Ca} > 0$, "steady" spheroid deformations and those predicted by the $O(\mathrm{Ca}^2)$ theory are visually indistinguishable, whereas for $\lambda = 10$ and $\mathrm{Ca} < 0$, the results of [32] "fall right in between" those for "steady" spheroids and for the BIE-based steady shapes from [51]; see Figure S2 *in the supplementary materials*. The deformation curves for "steady" spheroids obtained here and in [50, 51] are close for $D \in [-0.4, 0.3]$ but may deviate considerably for $D \notin [-0.4, 0.3]$ with the former being closer to the BIE-based results. There are two reasons for that: "steady" spheroids here and in [50, 51] minimize different kinematic condition errors (based on (8) and (24), respectively), and "steady" spheroid deformations here essentially follow from the inverse problem, whereas those in [50, 51] are the result of direct error minimization.

For each λ, Ca varies in a finite range $(\mathrm{Ca}_{\min}, \mathrm{Ca}_{\max})$ with $\mathrm{Ca}_{\max}$ and $\mathrm{Ca}_{\min}$ being critical values of Ca for extensional and compressional flows, respectively. When $\mathrm{Ca} \notin (\mathrm{Ca}_{\min}, \mathrm{Ca}_{\max})$, the drop either deforms indefinitely or disintegrates. Table 1 shows $\mathrm{Ca}_{\max}$ and $\mathrm{Ca}_{\min}$ and corresponding critical values of D, i.e., $D_{\max}$ and $D_{\min}$, respectively, predicted by $\mathrm{Ca} = \mathrm{Ca}^*(d)$ in (66) for various λ. Figures S3 and S4 *in the supplementary materials* compare $\mathrm{Ca}_{\max}$ and $\mathrm{Ca}_{\min}$ as functions of λ for "steady" spheroids and for BIE-based steady shapes [25, 51] and predicted by the $O(\mathrm{Ca}^2)$ theory [4] and by the slender body theory [35] ($\mathrm{Ca}_{\max} \sim 0.074\,\lambda^{-1/6}$ as $\lambda \to 0$). For further discussion of critical Ca, see *section* S4 *in the supplementary materials*.

5.2. Spheroidal drop under the presence of only uniform electric field. In the presence of the electric field only, $\mathrm{Ca} = 0$, and as a function of Ca_E, the Taylor deformation parameter D for "steady" spheroids (deformation curve) corresponds to the cross section of the deformation surface (65) at $\mathrm{Ca} = 0$. In the (Ca_E, D)-plane, it is plotted as $(\mathrm{Ca}_E^*((1+D)/(1-D)), D)$, where $\mathrm{Ca}_E^*(\cdot)$ is determined in (66). Figure 4 shows that the deformation curves for "steady" spheroids obtained here and in [54, Figs. 2 and 4] coincide visually for $(R, Q, \lambda) = (1.186 \cdot 10^{-3}, 3.0864, 13.643)$ (a drop of diglycidyl ether of bisphenol A (DGEBA) in a mixture of polysiloxanes and silicones

[10] Rallison [24, p. 62] remarked that the results of [25] (the dot-dashed curve in Figure 3) "have been superseded (for $\lambda = 1$) by numerical work of higher accuracy by B. R. Duffy and J. R. Blundell (unpublished), which agrees well with the quadratic theory of [4] over a larger range of Ca." In Figure 3 ($\lambda = 1$), deformations of the BIE-based steady shapes obtained by Duffy and Blundell and in [50] are much closer to those of the $O(\mathrm{Ca}^2)$ theory [4] than to those of the BIE-based shapes from [25].

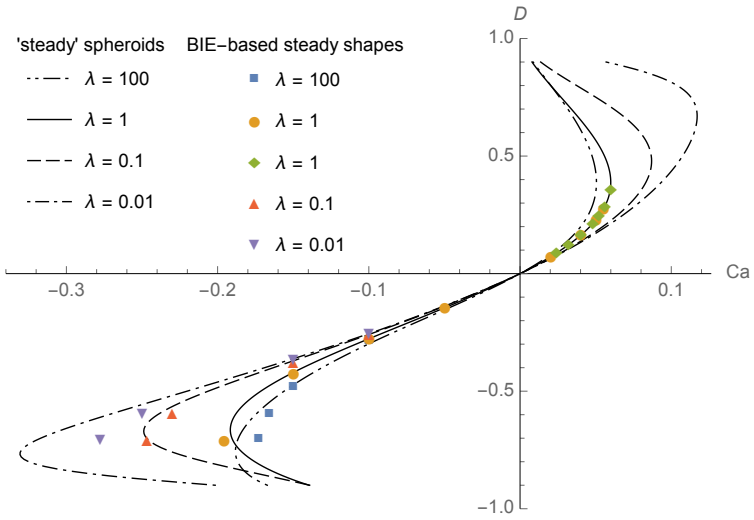

FIG. 2. *D for "steady" spheroids versus* Ca *(parametric plot* $(\mathrm{Ca}^*((D+1)/(D-1)), D)$ *with* $\mathrm{Ca}^*(\cdot)$ *determined by* (66)*) for* $\lambda = 0.01$, 0.1, 1, *and* 100. *For* $\mathrm{Ca} < 0$ *(compressional flow), triangles down, triangles up, circles, and squares correspond to BIE-based steady shapes for* $\lambda = 0.01$, 0.1, 1, *and* 100, *respectively, from* [51]. *For* $\mathrm{Ca} > 0$ *(extensional flow) and* $\lambda = 1$, *circles and diamonds correspond to those from* [50] *and to those from* [24, *Fig.* 6: *Duffy and Blundell*], *respectively.*

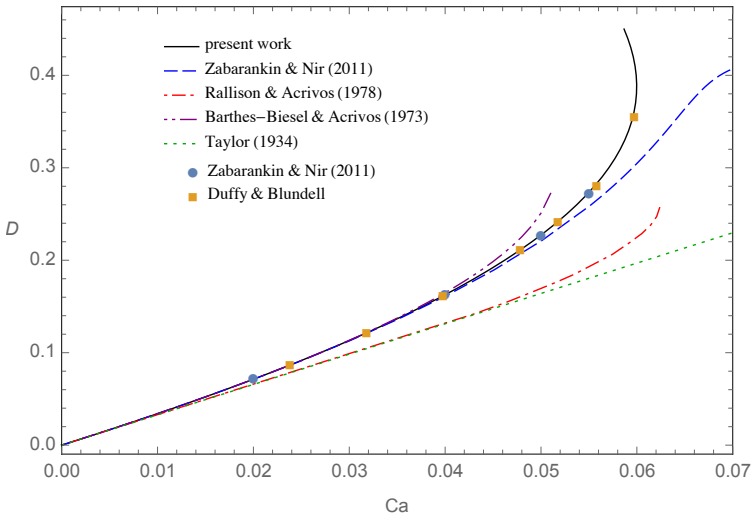

FIG. 3. *D versus* $\mathrm{Ca} \geqslant 0$ *for* $\lambda = 1$*: "steady" spheroids (solid curve, this work; dashed curve,* [50]*), BIE-based steady shapes (dot-dashed curve,* [25]*; circles,* [50]*; squares, Duffy and Blundell* [24, *Fig.* 6]*), the* $O(\mathrm{Ca})$ *theory* [34] *(dotted line), and the* $O(\mathrm{Ca}^2)$ *theory* [4] *(double-dot-dashed curve).*

TABLE 1

Critical values of the capillary number Ca *and of the Taylor deformation parameters D for "steady" spheroids in extensional* ($\mathrm{Ca} > 0$) *and compressional* ($\mathrm{Ca} < 0$) *flows for various* λ.

λ	0.01	0.1	0.5	1	2	10	100
$\mathrm{Ca}_{\max}$	0.1171	0.0870	0.0663	0.0600	0.0557	0.0516	0.0505
$\mathrm{Ca}_{\min}$	−0.3307	−0.2489	−0.202	−0.1916	−0.1871	−0.1869	−0.1882
$D_{\max}$	0.6698	0.479	0.4019	0.388	0.3833	0.3856	0.388
$D_{\min}$	−0.7661	−0.6706	−0.6475	−0.6645	−0.6906	−0.737	−0.7557

(PDMS)) and are quite close to each other and to the experimental data from [14] for $(R, Q, \lambda) = (0.03, 1.37, 0.874)$ (a castor oil drop in a silicon oil). Figure 4 also shows predictions of the $O(\mathrm{Ca}_E)$ and $O(\mathrm{Ca}_E^2)$ theories [37, 2] and of the ELDM [6]. Figures S7 and S8 *in the supplementary materials* compare "steady" spheroid deformations obtained based on (66) to those in [48], to the experimental results of Tsukada et al. [38] and of Vizika and Saville [40], to predictions of the $O(\mathrm{Ca}_E)$ and $O(\mathrm{Ca}_E^2)$ theories [37, 2] and of the ELDM [6], and to those of BIE-based steady shapes [17] for other triplets (R, Q, λ).

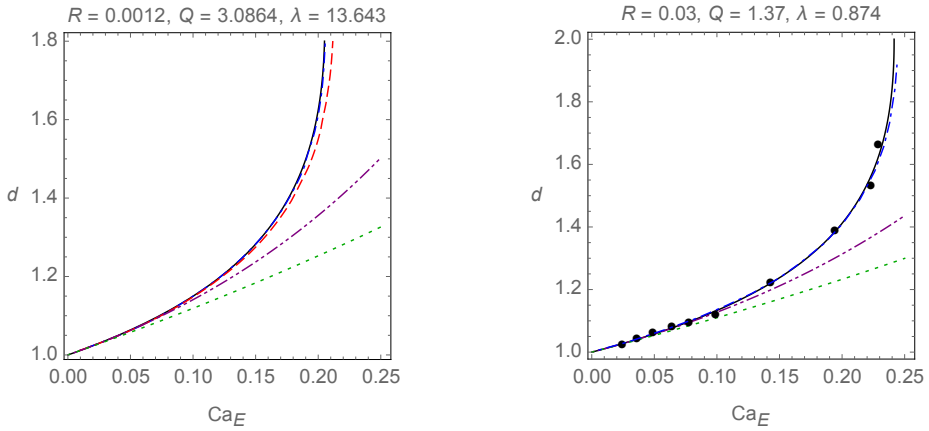

(a) drop of DGEBA in matrix of PDMS (b) castor oil drop in silicon oil

FIG. 4. *Drop's axes ratio d versus* Ca_E *for* (a) $(R, Q, \lambda) = (1.186 \cdot 10^{-3}, 3.0864, 13.643)$ *(drop of DGEBA in matrix of PDMS) and* (b) $(R, Q, \lambda) = (0.03, 1.37, 0.874)$ *(castor oil drop in silicon oil) for "steady" spheroids (solid curves, this work; dot-dashed curves,* [54, *Figs.* 2 *and* 4]*), the ELDM* [6] *(dashed curve in plot* (a)*), the* $O(\mathrm{Ca}_E^2)$ *theory* [2] *(double-dot-dashed curves), the* $O(\mathrm{Ca}_E)$ *theory* [37] *(dotted lines), and experimental data* [14] *(solid dots in plot* (b)*). In plot* (a)*, the solid and dot-dashed curves visually coincide.*

5.3. Spheroidal drop under presence of aligned linear flow and uniform electric field. In the case of aligned linear flow and a uniform electric field applied in combination, Figure 5 shows the deformation surface (65) for nine (R, Q, λ): $(10, 2, 1)$, $(0.5, 20, 1)$, $(0.1, 0.1, 0.05)$, $(0.1, 0.1, 20)$, $(10, 0.04, 1)$, $(0.04, 50, 0.05)$, $(0.04, 50, 20)$, $(0.016, 1.721, 14.71)$ and $(62.89, 0.581, 0.068)$. For the first seven (R, Q, λ), drop deformations were analyzed for "true" steady shapes [17] for $\mathrm{Ca} = 0$, whereas the eighth and ninth (R, Q, λ) correspond to a vegetable oil drop in a silicon oil medium and to a silicon oil drop in a vegetable oil medium and come from the experimental studies [38, 40] also for $\mathrm{Ca} = 0$. Any cross section of (65) at fixed D is a line, whereas the cross sections at $\mathrm{Ca}_E = 0$ and $\mathrm{Ca} = 0$ correspond to the deformation curves for the linear flow and electric field applied separately; see Figures 2 and 3 and Figures S7 and S8 *in the supplementary materials*, respectively. The shaded regions mark feasible $(\mathrm{Ca}, \mathrm{Ca}_E)$ satisfying (64).

Figure 6 and Figure S9 *in the supplementary materials* exemplify (Ca_E, D)-plane and (Ca, D)-plane projections of the deformation surface (65) for six (R, Q, λ): $(10, 0.04, 1)$, $(0.1, 0.1, 0.05)$, $(0.04, 50, 20)$, $(0.5, 20, 1)$, $(10, 2, 1)$, and $(62.89, 0.581, 0.068)$. In the first three cases, the electric field elongates the drop, and in the other three it compresses it. The dashed curves encompass the regions of feasible (Ca_E, D) and (Ca, D) satisfying (64), where the horizontal dashed lines at $D = 0$ correspond to

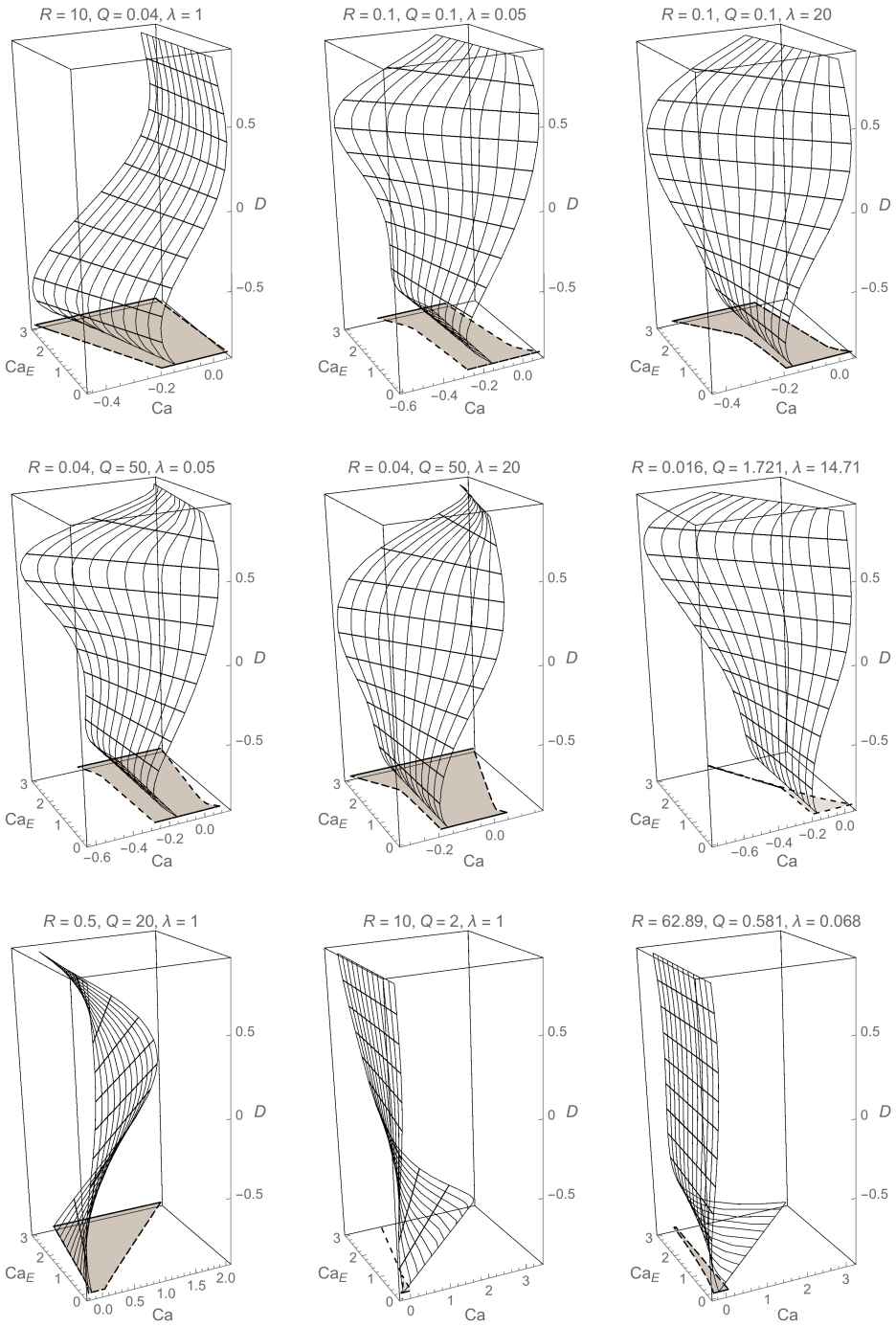

FIG. 5. *Deformation parameter* D *as a function of* Ca *and* Ca_E *(deformation surface* (65)*) for* (R, Q, λ) *shown on the top of each plot. The shaded regions mark feasible* $(\mathrm{Ca}, \mathrm{Ca}_E)$ *satisfying* (64).

a stationary sphere, for which the first condition in (31) holds. In the left and right plots, the contours that pass through $(0, 0)$ correspond to the deformation curves of the separately applied electric field (see Figures S7 and S8 *in the supplementary materials*) and liner flow (see Figures 2 and 3), respectively. For a detailed discussion of Figures 5, 6, and S9, see *section* S6 *in the supplementary materials*.

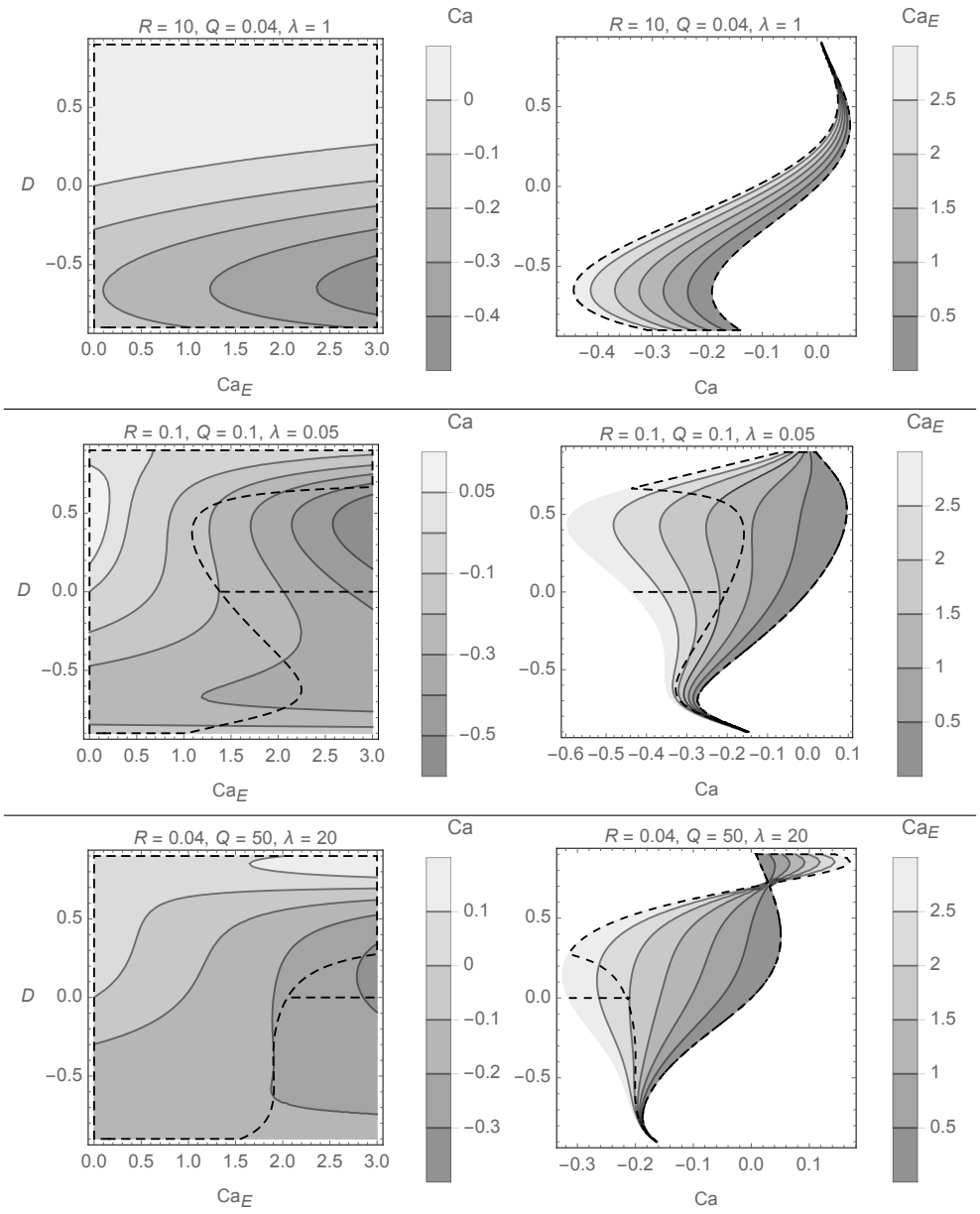

FIG. 6. *Projections of the deformation surface* (65) *onto the planes* (Ca_E, D) *and* (Ca, D) *for* $(R, Q, \lambda) = (10, 0.04, 1)$, $(0.1, 0.1, 0.05)$, *and* $(0.04, 50, 20)$. *The dashed curves encompass the regions of feasible* (Ca_E, D) *and* (Ca, D) *satisfying* (64). *The horizontal dashed lines at* $D = 0$ *correspond to a stationary sphere, for which the first condition in* (31) *holds.*

6. Conclusions. For an axisymmetric two-phase Stokes flow problem, stress boundary conditions (5) are recast as (17)–(19), and the problem is formulated in terms of the stream functions (25) satisfying the boundary conditions (23) and (26). For a spheroidal drop, (25) is represented by infinite series in the prolate spheroidal coordinates, and the coefficients in the series that satisfy exactly the velocity- and stress boundary conditions are determined analytically in the nonrecursive form (48) and (44). In contrast to the analytical solutions in [50, 51, 48], the obtained one is nonrecursive, whereas in contrast to those in [6, 54, 22], it satisfies exactly the velocity- and stress boundary conditions as well as the Stokes equations inside and outside the drop.

"Steady" spheroidal drops minimize the kinematic condition error (60). For $D \in [-0.5, 0.4]$ and all $\lambda = 0.01$, 0.1, 1, and 100, the coefficients f_k^γ and $\widehat{f}_k$, $k \geqslant 2$, in (58) are small compared to f_1^γ and $\widehat{f}_1$, respectively, which allows one to approximate the error (60) and to simplify optimality conditions. As a result, Ca, Ca_E, and D for "steady" spheroids are related by (67), where $\mathrm{Ca}^*(d)$ and $\mathrm{Ca}_E^*(d)$ are the capillary numbers that make a spheroidal drop with axes ratio d "steady" under separately applied linear flow and electric field, respectively, and $\mathrm{Ca}/\mathrm{Ca}^*(d)$ and $\mathrm{Ca}_E/\mathrm{Ca}_E^*(d)$ define relative strengths—the "percentage" that the linear flow and electric field contribute towards drop stability. For example, if the drop, being embedded in a linear flow with given Ca, is desired to be steady and to have certain axes ratio d, then this can be achieved by applying a uniform electric field with Ca_E found from (67) provided that $\mathrm{Ca}_E \geqslant 0$.

When $\mathrm{Ca}_E = 0$, the obtained deformation curves and critical values of Ca agree with the corresponding results for the BIE-based steady shapes obtained in [25, 32, 50, 51] and by Duffy and Blundell in [24] fairly well for $D \in [-0.5, 0.35]$ and are more accurate than those predicted by the $O(\mathrm{Ca}^2)$ theory and than those for "steady" spheroids from [50, 51]. When $\mathrm{Ca} = 0$, "steady" spheroid deformations, obtained here, are close to those for "steady" spheroids in [48, 54], are quite close to those for the BIE-based steady shapes [17] for $D \in [-0.5, 0.4]$, agree well with the $O(\mathrm{Ca}_E^2)$ theory [2] despite the discrepancy (74) in the quadratic terms, and are closer to the experimental data from [40, 38] than those predicted by the ELDM [6]. When $\mathrm{Ca} \neq 0$ and $\mathrm{Ca}_E > 0$, the deformation surface for "steady" spheroids is determined parametrically by (65) provided that $\mathrm{Ca}/\mathrm{Ca}_E \gtrless \widetilde{\mathscr{F}}(R, Q, \lambda)$ for $D \gtrless 0$, where $\widetilde{\mathscr{F}}(R, Q, \lambda)$ is defined by (29). Its qualitative behavior depends on the sign of $\mathscr{F}(R, Q, \lambda)$ and on whether $R \ll 1$, $R \sim 1$, or $R \gg 1$. For extended conclusions, see *section* S7 *in the supplementary materials.*

REFERENCES

[1] A. Acrivos and T. S. Lo, *Deformation and breakup of a single slender drop in an extensional flow*, J. Fluid Mech., 86 (1978), pp. 641–672.

[2] O. O. Ajayi, *A note on Taylor's electrohydrodynamic theory*, Proc. Roy. Soc. London Ser. A, 364 (1978), pp. 499–507.

[3] R. S. Allan and S. G. Mason, *Particle behaviour in shear and electric fields.* I. *Deformation and burst of fluid drops*, Proc. Roy. Soc. London Ser. A, 267 (1962), pp. 45–61.

[4] D. Barthès-Biesel and A. Acrivos, *Deformation and burst of a liquid droplet freely suspended in a linear shear field*, J. Fluid Mech., 61 (1973), pp. 1–21.

[5] O. A. Basaran and L. E. Scriven, *Axisymmetric shapes and stability of charged drops in an external electric field*, Phys. Fluids A, 1 (1989), pp. 799–809.

[6] N. Bentenitis and S. Krause, *Droplet deformation in DC electric fields: The extended leaky dielectric model*, Langmuir, 21 (2005), pp. 6194–6209.

[7] J. A. Champion, Y. K. Katare, and S. Mitragotri, *Particle shape: A new design parameter for micro- and nanoscale drug delivery carriers*, J. Contr. Release, 121 (2007), pp. 3–9.

[8] R. G. Cox, *The deformation of a drop in a general time-dependent fluid flow*, J. Fluid Mech.,

37 (1969), pp. 601–623.
[9] J. Q. Feng, *Electrohydrodynamic behavior of a drop subjected to a steady uniform electric field at finite electric Reynolds number*, Proc. Roy. Soc. London Ser. A, 455 (1999), pp. 2245–2269.
[10] J. Q. Feng and T. C. Scott, *A computational analysis of electrohydrodynamics of a leaky dielectric drop in an electric field*, J. Fluid Mech., 311 (1996), pp. 289–326.
[11] A. Fernandez, *Response of an emulsion of leaky dielectric drops immersed in a simple shear flow: Drops less conductive than the suspending fluid*, Phys. Fluids, 20 (2008), 043304.
[12] A. Fernandez, *Response of an emulsion of leaky dielectric drops immersed in a simple shear flow: Drops more conductive than the suspending fluid*, Phys. Fluids, 20 (2008), 043303.
[13] N. A. Frankel and A. Acrivos, *The constitutive equation for a dilute emulsion*, J. Fluid Mech., 44 (1970), pp. 65–78.
[14] J.-W. Ha and S.-M. Yang, *Deformation and breakup of Newtonian and non-Newtonian conducting drops in an electric field*, J. Fluid Mech., 405 (2000), pp. 131–156.
[15] J.-W. Ha and S.-M. Yang, *Electrohydrodynamic effects on the deformation and orientation of a liquid capsule in a linear flow*, Phys. Fluids, 12 (2000), pp. 1671–1684.
[16] J. Happel and H. Brenner, *Low Reynolds Number Hydrodynamics*, Springer, New York, 1983.
[17] E. Lac and G. M. Homsy, *Axisymmetric deformation and stability of a viscous drop in a steady electric field*, J. Fluid Mech., 590 (2007), pp. 239–264.
[18] L. G. Leal, *Laminar Flow and Convective Transport Processes*, Butterworth-Heinemann, Boston, 1992.
[19] J. R. Melcher and G. I. Taylor, *Electrohydrodynamics: A review of the role of interfacial shear stresses*, Annu. Rev. Fluid Mech., 1 (1969), pp. 111–146.
[20] M. J. Miksis, *Shape of a drop in an electric field*, Phys. Fluids, 24 (1981), pp. 1967–1972.
[21] V. Narsimhan, A. P. Spann, and E. S. G. Shaqfeh, *The mechanism of shape instability for a vesicle in extensional flow*, J. Fluid Mech., 750 (2014), pp. 144–190.
[22] H. Nganguia, Y.-N. Young, P. M. Vlahovska, J. Blawzdziewicz, J. Zhang, and H. Lin, *Equilibrium electro-deformation of a surfactant-laden viscous drop*, Phys. Fluids, 25 (2013), 092106.
[23] J. M. Rallison, *Note on the time-dependent deformation of a viscous drop which is almost spherical*, J. Fluid Mech., 98 (1980), pp. 625–633.
[24] J. M. Rallison, *The deformation of small viscous drops and bubbles in shear flows*, Annu. Rev. Fluid Mech., 16 (1984), pp. 45–66.
[25] J. M. Rallison and A. Acrivos, *A numerical study of the deformation and burst of a viscous drop in an extensional flow*, J. Fluid Mech., 89 (1978), pp. 191–200.
[26] C. E. Rosenkilde, *A dielectric fluid drop an electric field*, Proc. Roy. Soc. London Ser. A, 312 (1969), pp. 473–494.
[27] D. A. Saville, *Electrohydrodynamics: The Taylor-Melcher leaky dielectric model*, Annu. Rev. Fluid Mech., 29 (1997), pp. 27–64.
[28] J. D. Sherwood, *Spindle-shaped drops in a viscous extensional flow*, Math. Proc. Cambridge Philos. Soc., 90 (1981), pp. 529–536.
[29] J. D. Sherwood, *Breakup of fluid droplets in electric and magnetic fields*, J. Fluid Mech., 188 (1988), pp. 133–146.
[30] C. Sozou, *Electrohydrodynamics of a pair of liquid drops*, J. Fluid Mech., 67 (1975), pp. 339–348.
[31] H. A. Stone, *Dynamics of drop deformation and breakup in viscous fluids*, Annu. Rev. Fluid Mech., 26 (1994), pp. 65–102.
[32] H. A. Stone and L. G. Leal, *A note concerning drop deformation and breakup in biaxial extensional flows at low Reynolds numbers*, J. Colloid Interface Sci., 133 (1989), pp. 340–347.
[33] G. I. Taylor, *The viscosity of a fluid containing small drops of another fluid*, Proc. Roy. Soc. London Ser. A, 138 (1932), pp. 41–48.
[34] G. I. Taylor, *The formation of emulsions in definable fields of flow*, Proc. Roy. Soc. London Ser. A, 146 (1934), pp. 501–523.
[35] G. I. Taylor, *Conical free surfaces and fluid interfaces*, in Proceedings of the 11th International Congress on Applied Mechanics, Munich, 1964.
[36] G. I. Taylor, *Disintegration of water drops in an electric field*, Proc. Roy. Soc. London Ser. A, 280 (1964), pp. 383–397.
[37] G. I. Taylor, *Studies in electrohydrodynamics.* I. *The circulation produced in a drop by electrical field*, Proc. Roy. Soc. London Ser. A, 291 (1966), pp. 159–166.
[38] T. Tsukada, T. Katayama, Y. Ito, and M. Hozawa, *Theoretical and experimental studies of circulations inside and outside a deformed drop under a uniform electric field*, J. Chem.

Eng. Jpn., 26 (1993), pp. 698–703.
[39] A. F. Ulitko, *Vectorial Decompositions in the Three-Dimensional Theory of Elasticity*, Akademperiodika, Kiev, Ukraine, 2002.
[40] O. Vizika and D. A. Saville, *The electrohydrodynamic deformation of drops suspended in liquids in steady and oscillatory electric fields*, J. Fluid Mech., 239 (1992), pp. 1–21.
[41] P. M. Vlahovska, *On the rheology of a dilute emulsion in a uniform electric field*, J. Fluid Mech., 670 (2011), pp. 481–503.
[42] P. M. Vlahovska, D. Barthès-Biesel, and C. Misbah, *Flow dynamics of red blood cells and their biomimetic counterparts*, C. R. Phys., 14 (2013), pp. 451–458.
[43] P. M. Vlahovska, J. Blawzdziewicz, and M. Loewenberg, *Small-deformation theory for a surfactant-covered drop in linear flows*, J. Fluid Mech., 624 (2009), pp. 293–337.
[44] J. Walter, A.-V. Salsac, and D. Barthès-Biesel, *Ellipsoidal capsules in simple shear flow: Prolate versus oblate initial shapes*, J. Fluid Mech., 676 (2011), pp. 318–347.
[45] Y. Wu, A. Z. Zinchenko, and R. H. Davis, *General ellipsoidal model for deformable drops in viscous flows*, Ind. Eng. Chem. Res., 41 (2002), pp. 6270–6278.
[46] H. Yan, *Micro- and Nano-materials for Drug Delivery and Bioimaging Applications*, Ph.D. thesis, Kent State University, Kent, OH, 5 2015.
[47] E. Yariv and D. Rhodes, *Electrohydrodynamic drop deformation by strong electric fields: Slender-body analysis*, SIAM J. Appl. Math., 73 (2013), pp. 2143–2161, doi:10.1137/120880756.
[48] M. Zabarankin, *A liquid spheroidal drop in a viscous incompressible fluid under a steady electric field*, SIAM J. Appl. Math., 73 (2013), pp. 677–699, doi:10.1137/120888430.
[49] M. Zabarankin and P. Krokhmal, *Generalized analytic functions in 3D Stokes flows*, Quart. J. Mech. Appl. Math., 60 (2007), pp. 99–123.
[50] M. Zabarankin and A. Nir, *Generalized analytic functions in an extensional Stokes flow with a deformable drop*, SIAM J. Appl. Math., 71 (2011), pp. 925–951, doi:10.1137/100797370.
[51] M. Zabarankin, I. Smagin, O. M. Lavrenteva, and A. Nir, *Viscous drop in compressional Stokes flow*, J. Fluid Mech., 720 (2013), pp. 169–191.
[52] M. Zabarankin and A. F. Ulitko, *Hilbert formulas for r-analytic functions and Stokes flow about a biconvex lens*, Quart. Appl. Math., 64 (2006), pp. 663–693.
[53] M. Zabarankin and A. F. Ulitko, *Hilbert formulas for r-analytic functions in the domain exterior to spindle*, SIAM J. Appl. Math., 66 (2006), pp. 1270–1300, doi:10.1137/050632403.
[54] J. Zhang, J. D. Zahn, and H. Lin, *Transient solution for droplet deformation under electric fields*, Phys. Rev. E (3), 87 (2013), 043008.